Pergamon

Int. J. Solids Structures Vol. 33, No. 20–22, pp. 3103–3130, 1996
Copyright © 1996 Elsevier Science Ltd
Printed in Great Britain. All rights reserved
0020–7683/96 $15.00 + .00

0020–7683(95)00274–X

MULTISURFACE THERMOPLASTICITY FOR SINGLE CRYSTALS AT LARGE STRAINS IN TERMS OF EULERIAN VECTOR UPDATES

C. MIEHE
Institut für Mechanik (Bauwesen) Lehrstuhl I, Universität Stuttgart, 70569 Stuttgart, Pfaffenwaldring 7, Germany

Abstract—This paper presents a formulation of large-strain rate-independent multisurface thermoplasticity for single crystals and addresses aspects of its numerical implementation. The theoretical frame is the well-established continuum slip theory based on the multiplicative decomposition of the deformation gradient into elastic and plastic parts. A key feature of the present paper is the introduction and computational exploitation of a particularly simple hyperelastic stress response function based on a further multiplicative decomposition of the elastic deformation gradient into spherical and unimodular parts, resulting in a very convenient representation of the Schmid resolved shear stresses on the crystallographic slip systems in terms of a simple inner product of Eulerian vectors. This observation is intrinsically exploited on the numerical side by formulating a new fully implicit stress update algorithm and the associated consistent elastoplastic moduli in terms of these Eulerian vectors. The proposed return mapping algorithm treats the possibly redundant constraints of large-strain multisurface plasticity for single crystals by means of an active set search. Furthermore, it satisfies in an algorithmically exact way the plastic incompressibility condition in situations of multislip. The performance of the proposed formulation is demonstrated for two representative numerical simulations of thermoplastic deformation processes in single crystals with isotropic Taylor-type hardening. Copyright © 1996 Elsevier Science Ltd.

1. INTRODUCTION

This article presents a formulation of large-strain rate-independent multisurface thermoplasticity for single crystals and addresses aspects of its numerical implementation within a finite element analysis.

The so-called continuum slip theory for the phenomenological description of deformations in single crystals is well established in the literature. It assumes locally a multiplicative decomposition of the deformation gradient into a plastic part solely due to the plastic slip on crystallographic slip planes and an elastic part which describes lattice distortions and rigid rotations. This fundamental kinematic assumption, suggested from different points of view by Eckart (1948), Kröner (1964) and Lee (1969), serves as a basis for the definition of the local hyperelastic stress response in the single crystal. Theoretical frameworks of continuum single crystal plasticity have been outlined by Hill (1966), Kröner and Teodosiu (1972), Teodosiu (1970), Rice (1971), Mandel (1972), Teodosiu and Sidoroff (1976), Havner (1982a), Asaro (1983), see also the references therein. It is well known that single crystal plasticity can be recast into the mathematical framework of multisurface plasticity, as outlined for example in the works of Koiter (1960), Mandel (1972) and Maier (1970). In this format, the multiple constraints are the yield criterion functions on given crystallographic slip planes. In contrast to standard formulations of multisurface plasticity, these constraints can be linearly dependent and redundant. This results in a possible non-uniqueness of the set of active systems for a given deformation mode, see also Kocks (1970) and Havner (1982b) for a discussion of this point. In order to circumvent this problem, many authors have applied rate-dependent formulations based on power-type creep laws without division of slip systems into active and inactive sets via loading functions. These formulations have been applied as a numerical regularization technique, even in situations where rate-dependency is a physically negligible effect. We refer in this context to the

numerical implementations of rate-dependent single crystal plasticity documented in Peirce *et al.* (1982), Asaro and Needleman (1985), Needleman *et al.* (1985), Asaro and Needleman (1985) and the recent publications Mathur and Dawson (1989), Becker (1992), Kalidindi *et al.* (1992), Rashid and Nemat-Nasser (1992), Mohan *et al.* (1992), Cuitiño and Ortiz (1992), Steinmann and Stein (1996), see also the references therein. To the author's knowledge, the only work which treats rate-independent single crystal plasticity algorithmically in a consistent format of multisurface plasticity with redundant constraints are the recent publications by Borja and Wren (1992) and Cuitiño and Ortiz (1992).

The goal of this work on the theoretical side is to point out a simple constitutive structure of large-strain rate-independent elastoplasticity for monocrystals based on a particular choice of an isotropic hyperelastic stress response which governs the lattice distortions. As a key aspect, the deviatoric Kirchhoff stresses are assumed to be determined by a Neo-Hookean-type macroscopic free energy function formulated in terms of the unimodular part of the elastic deformation gradient. This simple model of isotropic elasticity, which implies a further multiplicative decomposition of the elastic deformation gradient into spherical and unimodular parts, has already been applied in formulations of polycrystal metal-elastoplasticity by several authors, see for example Simó and Miehe (1992). The main advantage of the model in the context of single crystal elastoplasticity is the extremely simple representation of the resolved shear stress which governs the plastic slip on a crystallographic slip system. This so-called Schmid stress assumes a representation in a Eulerian geometric setting similar to the geometric linear theory. It is proportional to the inner product of two Eulerian vectors, which are in turn images of the slip direction and slip plane normal on the isoclinic intermediate configuration, mapped by the unimodular part of the elastic deformation gradient.

This simple constitutive expression of the Schmid stress can be intrinsically exploited in the numerical implementation of the model. Here we propose as the main aspect of the paper a new fully implicit stress update algorithm for rate-independent crystal plasticity within a multisurface format. It turns out that this algorithm, as well as the closed form representation of the associated Eulerian consistent tangent moduli, appears in an extremely simple format when formulated in terms of the Eulerian vectors mentioned above. The stress update algorithm is based on a fully implicit backward Euler integrator of the plastic evolution equations, which can be recast into the elastic-predictor/plastic-corrector format of standard return maps in computational plasticity. The algorithm contains an active set search for the determination of the current slip systems parallel to the local Newton iteration. The concept is borrowed from nonlinear programming theory, see for example Luenberger (1984), and has been outlined for multisurface plasticity with linearly independent (non-redundant) constraints by Maier and Grieson (1979) and Simó *et al.* (1988), see also the references therein. The problem of non-uniqueness of the active set of slip systems due to redundant constraints is handled by setting up a *generalized inverse* of the possible overdetermined local system for the incremental slips which meets least-square-type optimality constraints. It is well known that a standard backward Euler algorithm does not satisfy the plastic incompressibility constraint in the case of multiple slip. We propose here an algorithmic extension which acts as a correcting postprocessor in a typical time step. Again, this procedure exploits in a crucial manner the particular form of the elasticity model for the deviatoric stress response. The key idea is to scale the trace of the algorithmic expression of the unimodular part of the elastic deformation gradient such that the plastic incompressibility constraint is satisfied.

Furthermore, the paper outlines a global solution algorithm for the coupled problem of single crystal thermoplasticity governed by the balance of linear momentum and the balance of energy. Staggered solution algorithms for the thermomechanically coupled global balance of momentum and energy have been proposed for example by Argyris and Doltsinis (1981) and Doltsinis (1990), based on iterative solution techniques for nonlinear equations, and for example by Simó and Miehe (1992), Armero and Simó (1992) and Miehe (1995) based on the methodology of operator splitting. We follow here the latter approach and apply a global solution algorithm for the coupled field equations of thermoplasticity based on an isothermal deformation predictor followed by a heat-conduction

corrector. This concept yields an algorithmic decomposition of the thermomechanical problem in a time step into two decoupled subproblems.

The paper is organized as follows. Section 2 lays out the constitutive framework of multiplicative multisurface thermoplasticity in a consistent mixed-variant geometric setting relative to the intermediate configuration. Section 3 presents the new constitutive stress update algorithm mentioned above and points out a closed form of the associated Eulerian consistent elastoplastic tangent moduli. Section 4 discusses some aspects of the global solution strategy and makes remarks concerning the finite element implementation. The paper concludes in Section 5 with two representative numerical examples which demonstrate the performance of the proposed formulation. Here we turn our attention to lattice rotations in the simple shear test and to shear band localization within the tension test.

2. MULTIPLICATIVE MULTISURFACE THERMOPLASTICITY

This section first of all summarizes some basics of multiplicative thermoplasticity for multisurface elastic domains. The underlying theoretical frame is straightforward and follows fundamental work such as Lee (1969), Teodosiu (1970), Rice (1971), Kröner and Teodosiu (1972), Mandel (1972) and Kratochvíl (1973). As a particular feature we point out here a canonical setting relative to the intermediate configuration in terms of mixed-variant tensor fields. This intrinsic representation of multiplicative elastoplasticity has been emphasised recently in Miehe and Stein (1992) and Miehe (1994b). The main contribution of this section is the specification of the framework mentioned above to a model of rate-independent single crystal thermoplasticity. This model is characterized by a particular isotropic hyperelastic stress response response, the compressible Neo-Hookean-type function first proposed by Flory (1963). The consequence of the application of this elasticity model is an extremely simple representation of the resolved Schmid stress on a typical slip system, which will be intrinsically exploited in the algorithmic treatment outlined in Section 3.

2.1. *Basic geometry of multiplicative elastoplasticity*

Let $\mathcal{B} \subset \mathbb{R}^3$ be the reference configuration of the body of interest and $\varphi_t(X): \mathcal{B} \to \mathbb{R}^3$ the nonlinear deformation map at time $t \in \mathbb{R}_+$. φ_t maps point $X \in \mathcal{B}$ of the reference configuration $\mathcal{B}$ onto points $x = \varphi_t(X) \in \varphi_t(\mathcal{B})$ of the current configuration. The deformation gradient $\mathbf{F}(X) := \nabla_X \varphi_t(X)$ with Jacobian $J(X) := \det[\mathbf{F}(X)] > 0$ maps tangent vectors of material curves onto tangent vectors of the deformed material curves. In the neighborhood of every $\mathbf{X} \in \mathcal{B}$ we consider the multiplicative decomposition

$$\mathbf{F} = \mathbf{F}^e \mathbf{F}^p \quad \text{with} \quad F^a{}_A = F^{ea}{}_{\bar{A}} F^{p\bar{A}}{}_A \tag{1}$$

of the linear tangent map $\mathbf{F}$ into an elastic part $\mathbf{F}^e$ and a plastic part $\mathbf{F}^p$. $\mathbf{F}^p$ defines *locally* a macro-stress-free plastic intermediate configuration and is assumed to be determined by a constitutive assumption for the evolution $\dot{\mathbf{F}}^p := (\partial/\partial t)\mathbf{F}^p$ with initial condition $\mathbf{F}^p_t(t = t_0) = \mathbf{1}$ at the reference configuration. In the context of single crystal plasticity, $\mathbf{F}^p$ describes the part of the local deformations *solely* due to the plastic slip on crystallographic planes. The part $\mathbf{F}^e$ contains the lattice deformation and local rigid body rotations.

For the subsequent development we consider the multiplicative splits of the mappings defined in eqn (1) into spherical and unimodular parts

$$\mathbf{F} := J^{1/3} \bar{\mathbf{F}}; \quad \mathbf{F}^e := J^{e1/3} \bar{\mathbf{F}}^e; \quad \mathbf{F}^p := J^{p1/3} \bar{\mathbf{F}}^p. \tag{2}$$

The Jacobians $J := \det[\mathbf{F}]$, $J^e := \det[\mathbf{F}^e]$ and $J^p := \det[\mathbf{F}^p]$ are associated with the volumetric total, elastic and plastic part of the deformation. The unimodular parts $\bar{\mathbf{F}}$, $\bar{\mathbf{F}}^e$ and $\bar{\mathbf{F}}^p$ with unit determinant contain isochoric contributions.

Let $\mathbf{l} = \nabla_x \mathbf{v} = \dot{\mathbf{F}}\mathbf{F}^{-1}$ with the component representation $l^a{}_b = \dot{F}^a{}_R F^{-1R}{}_b$ denote the spatial velocity gradient. The consistent transformation of this mixed-variant tensor field

to the intermediate configuration is a composition with the partial tangent map $\mathbf{F}^e$ defined in eqn (1) and can be additively decomposed into pure elastic and pure plastic parts

$$\underbrace{\mathbf{F}^{e-1}\dot{\mathbf{F}}^e}_{\mathbf{L}} = \underbrace{\mathbf{F}^{e-1}\dot{\mathbf{F}}^e}_{\mathbf{L}^e} + \underbrace{\dot{\mathbf{F}}^p\mathbf{F}^{p-1}}_{\mathbf{L}^p}, \tag{3}$$

see Miehe (1994b). The elastic and plastic parts of these mixed-variant tensor fields relative to the intermediate configuration can be further decomposed into spherical and deviatoric contributions based on the decompositions (2)

$$\mathbf{L}^e = \frac{\dot{J}^e}{J^e}\frac{1}{3}\mathbf{1} + \bar{\mathbf{F}}^{e-1}\dot{\bar{\mathbf{F}}}^e \quad \text{and} \quad \mathbf{L}^p = \frac{\dot{J}^p}{J^p}\frac{1}{3}\mathbf{1} + \dot{\bar{\mathbf{F}}}^p\bar{\mathbf{F}}^{p-1}. \tag{4}$$

Let $\tau = \tau^{ab}$ denote the contravariant Eulerian–Kirchhoff stress tensor. Then $\mathbf{g}\tau = \delta_{ar}\tau^{rb}$ is work-conjugate to $\mathbf{l} = l^a{}_b$. The composition of this mixed-variant Eulerian stress field with the partial tangent map $\mathbf{F}^e$ in eqn (1) gives the stress tensor $\mathbf{\Sigma} = \Sigma_{\bar{A}}{}^{\bar{B}}$ work-conjugate to $\mathbf{L} = L^{\bar{A}}{}_{\bar{B}}$ defined in eqn (3). Thus we write the stress power per unit of the reference configuration

$$\mathscr{P} := \mathbf{\Sigma} : \mathbf{L} \quad \text{with} \quad \mathbf{\Sigma} := \mathbf{F}^{eT}[\mathbf{g}\tau]\mathbf{F}^{e-T} \tag{5}$$

in the geometric representation relative to the intermediate configuration.

2.2. *Isotropic thermoelastic stress response*

2.2.1. *Free energy function.* The thermoelastic response of the crystalline solid is governed by the lattice deformation and by local inhomogeneous deformation fields due to dislocations and point defects. Thus, we assume a dependence of the free energy

$$\psi = \hat{\psi}(\mathbf{F}^e, A, \vartheta) \tag{6}$$

on the lattice deformation $\mathbf{F}^e$, a strain-like internal variable A which describes on average the local inhomogeneous deformation fields and the absolute temperature ϑ. In crystalline materials it is often assumed that the micro-stress fields do not affect the macro-stress fields. This observation is consistent with an additive decomposition of the free energy

$$\psi = \hat{\psi}_{\text{macro}}(\mathbf{F}^e, \vartheta) + \hat{\psi}_{\text{micro}}(\mathbf{A}, \vartheta) \tag{7}$$

into decoupled macroscopic and microscopic parts. Furthermore, it makes sense to decompose the macroscopic part of the free energy into decoupled contributions associated with the volumetric and isochoric part of the deformation. Based on the decomposition eqn (2) we assume

$$\psi = \hat{\psi}^{\text{vol}}_{\text{macro}}(\mathbf{J}^e, \vartheta) + \hat{\psi}^{\text{iso}}_{\text{macro}}(\bar{\mathbf{F}}^e, \vartheta) + \hat{\psi}_{\text{micro}}(\mathbf{A}, \vartheta), \tag{8}$$

where the volumetric part $\psi^{\text{vol}}_{\text{macro}}$ is assumed to contain the pure thermal contribution, i.e., the heat capacity part of the free energy. Note that the functions (6)–(8) have to satisfy the principle of material frame invariance, for example $\hat{\psi}(\mathbf{Q}\mathbf{F}^e, A, \vartheta) = \hat{\psi}(\mathbf{F}^e, A, \vartheta)$ for all $\mathbf{Q} \in SO(3)$, where $SO(3)$ denotes the proper orthogonal group.

2.2.2. *Hyperelastic stress functions.* The so-called Clausius–Planck inequality for the internal plastic dissipation per unit of the reference volume can be written in the form

Table 1. Multiplicative multisurface thermoplasticity

		Isotropic thermoelasticity:
(1)	*free energy*	$\psi = \hat{\psi}^{\text{vol}}_{\text{macro}}(J^{\text{e}}, \vartheta) + \hat{\psi}^{\text{iso}}_{\text{macro}}(\bar{\mathbf{F}}^{\text{e}}, \vartheta) + \hat{\psi}_{\text{micro}}(A, \vartheta)$
(2)	macro-stress	$\boldsymbol{\Sigma} = J^{\text{e}}\, \partial_{J^{\text{e}}} \hat{\psi}^{\text{vol}}_{\text{macro}} \mathbf{1} + \text{dev}\,[\bar{\mathbf{F}}^{\text{eT}}\, \partial_{\mathbf{F}^{\text{e}}} \hat{\psi}^{\text{vol}}_{\text{macro}}]$
(3)	micro-stress	$B = \partial_{\text{A}} \hat{\psi}_{\text{micro}}$
(4)	entropy	$\eta = -\partial_{\vartheta}(\hat{\psi}^{\text{vol}}_{\text{macro}} + \hat{\psi}^{\text{iso}}_{\text{macro}} + \hat{\psi}_{micro})$
		Isochoric multi-surface thermoplasticity:
(5)	*flow criterion*	$\phi^{\alpha} = \hat{\phi}^{\alpha}_{\text{macro}}(\text{dev}\,[\boldsymbol{\Sigma}]) - \hat{\phi}_{\text{micro}}(B, \vartheta)$
(6)	flow rule	$\mathbf{L}^{\text{p}} = \sum_{\alpha=1}^{m} \lambda^{\alpha}\, \text{dev}\,[\partial_{\text{dev}[\boldsymbol{\Sigma}]} \hat{\phi}^{\alpha}_{\text{macro}}]$
(7)	evolution	$\dot{A} = \sum_{\alpha=1}^{m} \lambda^{\alpha}\, \partial_{\text{B}} \hat{\phi}_{\text{micro}}$
(8)	loading	$\lambda^{\alpha} \geqslant 0,\ \hat{\phi}^{\alpha} \leqslant 0,\ \lambda^{\alpha} \phi^{\alpha} = 0$

$$\mathscr{D}^{\text{p}} := \boldsymbol{\Sigma} : \mathbf{L} - \eta \dot{\vartheta} - \dot{\psi} \geqslant 0 \tag{9}$$

based on the expression for the stress power relative to the intermediate configuration defined in eqn (5). η denotes the entropy field. Taking into account the evolution of the free energy based on the constitutive assumption above

$$\begin{aligned} \dot{\psi} &= \mathbf{F}^{\text{eT}}\, \partial_{\mathbf{F}^{\text{e}}} \hat{\psi} : \mathbf{L}^{\text{e}} + \partial_{\text{A}} \hat{\psi} \dot{\text{A}} + \partial_{\vartheta} \hat{\psi} \dot{\vartheta} \\ &= \{J^{\text{e}}\, \partial_{J^{\text{e}}} \psi^{\text{vol}}_{\text{macro}} \mathbf{1} + \text{dev}\,[\bar{\mathbf{F}}^{\text{eT}}\, \partial_{\mathbf{F}^{\text{e}}} \hat{\psi}^{\text{vol}}_{\text{macro}}]\} : \mathbf{L}^{\text{e}} + \partial_{\text{A}} \hat{\psi}_{\text{micro}} \dot{\text{A}} \\ &\quad + \partial_{\vartheta}(\hat{\psi}^{\text{vol}}_{\text{macro}} + \hat{\psi}^{\text{iso}}_{\text{macro}} + \hat{\psi}_{\text{micro}}) \dot{\vartheta}, \end{aligned} \tag{10}$$

we obtain, based on standard arguments, the hyperelastic equations for the stresses and the entropy in Table 1. The insertion of these results into eqn (9) yields the reduced dissipation equation

$$\mathscr{D}^{\text{p}} := \boldsymbol{\Sigma} : \mathbf{L}^{\text{p}} - B\dot{A} \geqslant 0. \tag{11}$$

2.3. *Evolution equations for multisurface plastic flow*

2.3.1. *Flow criterion function.* In the framework of multisurface plasticity we consider at a given temperature ϑ a non-smooth convex elastic domain in the stress space

$$\mathbb{E}_{\vartheta} := \{(\boldsymbol{\Sigma}, B) \mid \hat{\phi}^{\alpha}(\boldsymbol{\Sigma}, B, \vartheta) \leqslant 0 \quad \text{for} \quad \alpha = 1, 2, \ldots, m\} \tag{12}$$

based on m independent flow criterion functions

$$\phi = \hat{\phi}^{\alpha}(\boldsymbol{\Sigma}, B, \vartheta). \tag{13}$$

These functions relate the current stress to a temperature-dependent material function in the form

$$\phi = \hat{\phi}^{\alpha}_{\text{macro}}(\boldsymbol{\Sigma}) - \hat{\phi}_{\text{micro}}(B, \vartheta). \tag{14}$$

We restrict our considerations in what follows to isochoric plasticity and assume the plastic flow to be independent of the hydrostatic macro-stress state. This is consistent with the formulation

Table 2. Model problem. Multislip single-crystal thermoplasticity

		Isotropic thermolelasticity:
(1)	*free energy*	$\psi = \frac{1}{2}\kappa \ln^2[J^e] - \kappa\delta \ln[J^e](\vartheta-\vartheta_0) + c(\vartheta-\vartheta_0-\vartheta\ln[\vartheta/\vartheta_0]) + \frac{1}{2}\mu(\bar{\mathbf{F}}^e:\bar{\mathbf{F}}^e-3)+\hat{\psi}_{\text{micro}}(A,\vartheta)$
(2)	macro-stress	$\boldsymbol{\Sigma} = (\kappa \ln[J^e] - \kappa\delta(\vartheta-\vartheta_0))\mathbf{1} + \mu \operatorname{dev}[\bar{\mathbf{F}}^{e\mathrm{T}}\bar{\mathbf{F}}^e]$
(3)	micro-stress	$B = \partial_A\hat{\psi}_{\text{micro}}(A,\vartheta)$
(4)	entropy	$\eta = \ln[\vartheta/\vartheta_0] + \kappa\delta \ln[J^e] - \partial_\vartheta\hat{\psi}_{\text{micro}}(A,\vartheta)$
		Multislip thermoplasticity:
(5)	*flow criterion*	$\phi^\alpha = \tau^\alpha - [\hat{\tau}_0(\vartheta) + \hat{B}(A,\vartheta)]$ with $\tau^\alpha := \boldsymbol{\Sigma}:(\mathbf{S}^\alpha \otimes \mathbf{M}^\alpha)$
(6)	flow rule	$\mathbf{L}^p = \Sigma_{\alpha=1}^m \lambda^\alpha \mathbf{S}^\alpha \otimes \mathbf{M}^\alpha$
(7)	evolution	$\dot{A} = \Sigma_{\alpha=1}^m \lambda^\alpha$
(8)	loading	$\lambda^\alpha \geqslant 0, \quad \hat{\phi}^\alpha \leqslant 0, \quad \lambda^\alpha\hat{\phi}^\alpha = 0$

$$\phi = \hat{\phi}^\alpha_{\text{macro}}(\operatorname{dev}[\boldsymbol{\Sigma}]) - \hat{\phi}_{\text{micro}}(B,\vartheta). \tag{15}$$

2.3.2. *Associative evolution equations.* Based on the above assumption we derive the canonical associative evolution equations together with the non-isothermal loading-unloading condition from the argument

$$[\boldsymbol{\Sigma} - \overset{*}{\boldsymbol{\Sigma}}]:\mathbf{L}^p - [B - \overset{*}{B}]\dot{A} \geqslant 0 \;\forall\; \{\overset{*}{\boldsymbol{\Sigma}}, \overset{*}{B}\} \in \mathbb{E}_\vartheta \tag{16}$$

for all admissible variations $\{\overset{*}{\boldsymbol{\Sigma}}, \overset{*}{B}\}$ of the stresses. This implies the normality rules in Table 1 for the plastic flow $\mathbf{L}^p$ and the evolution $\dot{A}$ of the internal variable along with the non-isothermal loading-unloading conditions. These equations follow as the Kuhn–Tucker equations from the Lagrangian associated with the constraint maximization problem (16) based on standard arguments of convex analysis. Observe that the plastic flow rule is, based on assumption eqn (15), purely deviatoric and therefore preserves the plastic volume, i.e., we have $J^p = 0$ in eqn $(4)_2$. This consideration completes the constitutive set of multiplicative thermoplasticity in the mixed-variant geometric setting relative to the intermediate configuration.

2.4. *Model problem. Multislip monocrystal thermoplasticity*

As a typical model problem of large-strain multisurface thermoplasticity we now consider a formulation of monocrystal plasticity. The specification of the constitutive functions is given in Table 2. The isotropic macroscopic contributions to the free energy are determined by a volumetric deformation term, an isochoric deformation term of the Neo-Hookean type and a heat capacity term. It is determined by the material constants $\kappa > 0$, $\mu > 0$, $\delta > 0$ and $c > 0$ which denote the bulk modulus, the shear modulus, the thermal expansion coefficient and the heat capacity at a given absolute reference temperature ϑ_0, respectively. The microscopic part of the free energy which governs the temperature-dependent hardening behaviour will be specified in Section 5.

The flow criterion function ϕ^α are formulated in terms of the Schmid resolved shear stresses

$$\tau^\alpha := \operatorname{dev}[\boldsymbol{\Sigma}]:(\mathbf{S}^\alpha \otimes \mathbf{M}^\alpha) \tag{17}$$

on the slip system α. The slip system is defined by the two orthonormal vectors $(\mathbf{S}^\alpha, \mathbf{M}^\alpha)$ which define the slip direction and the slip-plane normal. Observe the particularly simple constitutive formulation of the Schmid stress based on the Neo-Hookean type model for the isotropic stress deviator

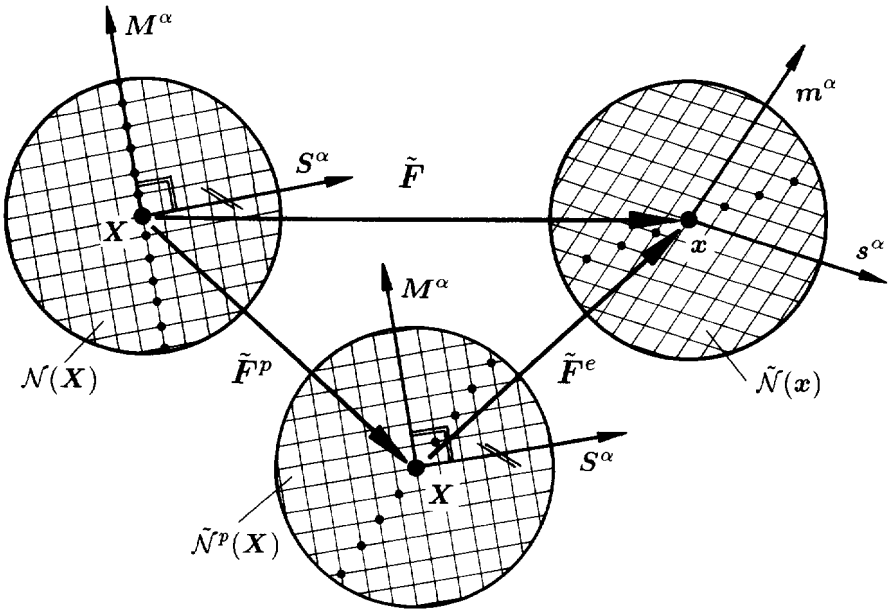

Fig. 1. Geometry of a single slip system (α). The orthonormal Lagrangian unit vectors ($\mathbf{S}^\alpha, \mathbf{M}^\alpha$) at the isoclinic intermediate configuration are transformed by the unimodular map $\tilde{\mathbf{F}}^e$ onto the Eulerian vectors ($\mathbf{s}^\alpha, \mathbf{m}^\alpha$). The Schmid stress of the elastically isotropic material under consideration is then simply defined as $\tau^\alpha = \mu \mathbf{s}^\alpha \cdot \mathbf{m}^\alpha$.

$$\tau^\alpha = \mu \mathbf{s}^\alpha \cdot \mathbf{m}^\alpha \quad \text{with} \quad \mathbf{s}^\alpha := \tilde{\mathbf{F}}^e \mathbf{S}^\alpha \quad \text{and} \quad \mathbf{m}^\alpha := \tilde{\mathbf{F}}^e \mathbf{M}^\alpha. \tag{18}$$

Thus the pairs of Eulerian vectors ($\mathbf{s}^\alpha, \mathbf{m}^\alpha$) of the slip systems are obtained by mapping the orthonormal vectors ($\mathbf{S}^\alpha, \mathbf{M}^\alpha$) of the slip system by the unimodular part $\tilde{\mathbf{F}}^e$ of the elastic deformation gradient, see Fig. 1. The Schmid stress τ^α of the slip system α is then simply proportional to the inner product of the Eulerian vectors ($\mathbf{s}^\alpha, \mathbf{m}^\alpha$). This simple representation will be intrinsically exploited in the numerical treatment where the return algorithm can be formulated in terms of simple vector updates.

The flow rule for $\mathbf{L}^p$ in Table 2 is deviatoric and determined by the slip rate λ^α on each slip system. The evolution $\dot{A}$ of the internal variable A, which describes on average the micro deformation fields, turns out to be the sum of the slip rates λ^α on all slip systems. Thus the model under consideration is consistent with so-called isotropic Taylor hardening. The insertion of the evolution equations in Table 2 into eqn (11) yields, taking into account the loading-unloading conditions, the expression

$$\mathscr{D}^p = \sum_{\alpha=1}^{m} (\tau^\alpha - B)\lambda^\alpha = \hat{\tau}_0(\vartheta)\dot{A} \geqslant 0 \tag{19}$$

for the internal dissipation of the model problem under consideration.

3. INTEGRATION ALGORITHM FOR THE LOCAL EVOLUTION EQUATIONS

We now propose a new constitutive integration algorithm for the rate-independent model of single crystal plasticity summarized in Table 2. The algorithm relies intrinsically on the simple representation of the resolved shear stress τ^α and results in an iterative treatment of the Eulerian vectors ($\mathbf{s}^\alpha, \mathbf{m}^\alpha$) defined in eqn (18). The underlying basis is a fully implicit backward Euler integrator applied to the deviatoric part of the plastic evolution operator $(4)_2$. This scheme is known to be absolutely stable and first-order accurate. In order to satisfy the constraints of multisurface plasticity we apply ideas from nonlinear programming techniques. That results in an iterative treatment of the current slip systems in an active set strategy.

It is well known that a backward Euler scheme does not satisfy the plastic incompressibility constraint in the presence of multislip. We therefore propose an algorithmic overlay which exactly preserves the plastic volume in each incremental step. Again, this postprocessor relies critically on the additive decomposition of the hyperelastic stress response into decoupled volumetric and isochoric contributions. The section concludes with the derivation of the algorithmic elastoplastic moduli which appear in a remarkably simple format within the Eulerian geometric setting.

3.1. *Backward-Euler integrator of evolution equations*

Consider a time interval $[t_n, t_{n+1}] \in \mathbb{R}_+$ and assume that all variables at time t_n are known. Then a standard backward Euler integrator of the evolution equations for $\mathrm{dev}[\mathbf{L}^p] = \dot{\tilde{\mathbf{F}}}^p \tilde{\mathbf{F}}^{p-1}$ and $\dot{A}$ in Table 2 gives the system

$$\left.\begin{aligned} \tilde{\mathbf{F}}^p &= \tilde{\mathbf{F}}^p_n + \sum_{\alpha=1}^{m} \gamma^\alpha (\mathbf{S}^\alpha \otimes \mathbf{M}^\alpha) \tilde{\mathbf{F}}^p \\ A &= A^* + \sum_{\alpha=1}^{m} \gamma^\alpha \\ \gamma^\alpha &\geqslant 0, \hat{\phi}^\alpha \leqslant 0, \gamma^\alpha \hat{\phi}^\alpha = 0 \end{aligned}\right\}. \tag{20}$$

After some straightforward algebraic manipulations based on $\tilde{\mathbf{F}} = \tilde{\mathbf{F}}^e \tilde{\mathbf{F}}^p$ we end up with the alternative representation

$$\left.\begin{aligned} \tilde{\mathbf{F}}^e &= \tilde{\mathbf{F}}^{e*} - \sum_{\alpha=1}^{m} \gamma^\alpha \mathbf{s}^{\alpha*} \otimes \mathbf{M}^\alpha \\ A &= A^* + \sum_{\alpha=1}^{m} \gamma^\alpha \\ \gamma^\alpha &\geqslant 0, \hat{\phi}^\alpha \leqslant 0, \gamma^\alpha \hat{\phi}^\alpha = 0 \end{aligned}\right\} \tag{21}$$

in terms of the *elastic predictor* state values

$$\tilde{\mathbf{F}}^{e*} := \tilde{\mathbf{F}} \tilde{\mathbf{F}}^{p-1}_n; \quad A^* := A_n; \quad \mathbf{s}^{\alpha*} := \tilde{\mathbf{F}}^{e*} \mathbf{S}^\alpha; \quad \mathbf{m}^{\alpha*} := \tilde{\mathbf{F}}^{e*} \mathbf{M}^\alpha. \tag{22}$$

All variables without subscript are assumed to be evaluated at time t_{n+1}. $\gamma^\alpha := \lambda^\alpha_{n+1}(t_{n+1} - t_n)$ denote the incremental plastic parameters on the slip system α. Observe that, in the case of plastic multislip, the algorithms $(20)_1$ and $(21)_1$ do not satisfy the constraints $\det[\tilde{\mathbf{F}}^p] = 1$ and $\det[\tilde{\mathbf{F}}^e] = 1$, respectively. We comment on this point in Section 3.4.

Based on the fact that the elastic domain $\mathbb{E}_\vartheta$ defined in eqn (12) is convex, we can decide the plastic loading in a typical time increment in terms of the trial state values. For

$$\phi^{\alpha*} = \mu \mathbf{s}^{\alpha*} \cdot \mathbf{m}^{\alpha*} - \hat{y}(A^*, \vartheta) \leqslant 0 \quad \text{for all} \quad \alpha \in \mathcal{S} \tag{23}$$

the step is elastic. If only one flow criterion function is violated in the sense $\phi^{\alpha*} > 0$, the associated incremental step is elastic–plastic. In the equation above,

$$\mathcal{S} := \{1, \ldots, m\} \tag{24}$$

denotes the *set of possible slip systems*. As an example we have $m = 2 \times 12$ slip systems for f.c.c. crystals when differentiating between positive and negative slip directions. For the

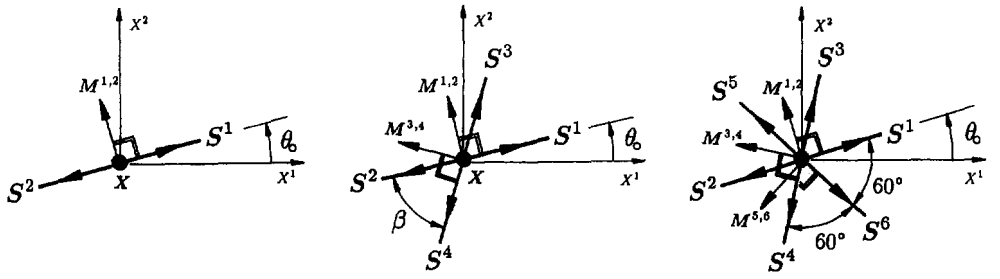

a. Single Slip System b. Double Slip Model c. Equilateral Triangle Model

Fig. 2. Idealized plane slip models with initial orientation θ relative to the Cartesian frame of the reference configuration. (a) Single slip system, (b) Asaro's double slip model with fixed relative orientation β, (c) closest package idealized plane slip model with three slip systems arranged in an equilateral triangle.

three simplified plane arrangements depicted in Fig. 2(a–c) we have $m = 2\times 2, 2\times 4, 2\times 6$, respectively.

3.2. *Return-mapping algorithm in terms of Eulerian vector updates*

If flow criterion functions for some $\alpha\in\mathscr{S}$ are violated in the sense $\phi^{\alpha *} > 0$, we have to restore plastic consistency. We now face the problem that the set $\mathscr{A}\subset\mathscr{S}$ of active constraints with $\gamma^\alpha > 0$ and $\phi^\alpha = 0$ for $\alpha\in\mathscr{A}$ at the end of the time interval is not *a priori* known. It is not uniquely determined by the trial state (22). Thus we have to perform a search for the active set $\mathscr{A}$ by means of an iterative procedure. The terminology of such search algorithms is usually borrowed from the theory of convex nonlinear programming, see, e.g., Luenberger (1984). Algorithmic treatments of multisurface plasticity on this basis have been proposed, e.g., by Maier (1970) and Simó *et al.* (1988) for the case of linearly independent (non-redundant) constraints, see also the references therein. Applications of active set algorithms for single crystal plasticity with possible linearly dependent (redundant) constraints have been suggested recently by Borja and Wren (1993) for the small-strain format and by Cuitiño and Ortiz (1992) for the large-strain setting. We here extend conceptually ideas discussed in Borja and Wren (1993) to the large-strain format and solve the Kuhn–Tucker-type loading-unloading conditions $(21)_{3-5}$ by means of the following iterative procedure.

Based on the trial state introduced above we make a first estimate for the *active working set*

$$\mathscr{A} = \{\alpha\in\mathscr{S} \mid \phi^{\alpha *} > \mathrm{tol}_\phi\}, \tag{25}$$

where $\mathrm{tol}_\phi\in\mathbb{R}_+$ is a small machine-dependent tolerance value. Then we initialize $\gamma^\alpha = 0$ for all $\alpha\in\mathscr{S}$ and compute for $\alpha\in\mathscr{A}$ the actual incremental plastic parameters γ^α from the associated consistency conditions $(21)_5$. Therefore based on $(21)_1$ we first express the actual Eulerian vectors $(\mathbf{s}^\alpha, \mathbf{m}^\alpha)$ in eqn (18) in terms of the trial Eulerian vectors $(\mathbf{s}^{\alpha *}, \mathbf{m}^{\alpha *})$ defined in eqn (22)

$$\mathbf{s}^\alpha = \mathbf{s}^{\alpha *} - \sum_{\beta\in\mathscr{A}} \gamma^\beta \mathbf{s}^{\beta *} S^{\beta\alpha} \quad \text{and} \quad \mathbf{m}^\alpha = \mathbf{m}^{\alpha *} - \sum_{\beta\in\mathscr{A}} \gamma^\beta \mathbf{s}^{\beta *} M^{\beta\alpha}, \tag{26}$$

introducing the constant matrices

$$S^{\beta\alpha} := \mathbf{M}^\beta \cdot \mathbf{S}^\alpha \quad \text{and} \quad M^{\beta\alpha} := \mathbf{M}^\beta \cdot \mathbf{M}^\alpha. \tag{27}$$

With these definitions in hand, we can formulate the flow criterion functions

$$\phi^\alpha = \mu[S^{\alpha *} - \sum_{\beta \in \mathscr{A}} \gamma^\beta \mathbf{s}^{\beta *} S^{\beta\alpha}] \cdot [\mathbf{m}^{\alpha *} - \sum_{\delta \in \mathscr{A}} \gamma^\delta \mathbf{s}^{\delta *} M^{\delta\alpha}] - \hat{y}(A^* + \sum_{\varepsilon \in \mathscr{A}} \gamma^\varepsilon, \vartheta) \tag{28}$$

exclusively in terms of the Eulerian trial state vectors and the incremental plastic parameters γ^α. The solution of the consistency conditions $\phi^\alpha = 0$ for the plastic parameters γ^α is performed by a local Newton iteration based on the linearization of eqn (28), leading to the update

$$\gamma^\alpha \Leftarrow \gamma^\alpha + \sum_{\beta \in \mathscr{A}} G^{\alpha\beta -1} \phi^\beta \quad \text{with} \quad G^{\alpha\beta} := -\frac{\partial \phi^\alpha}{\partial \gamma^\beta} \quad \text{for} \quad (\alpha, \beta) \in \mathscr{A}. \tag{29}$$

The coefficients of the Jacobian $G^{\alpha\beta}$ can be computed in a straightforward manner from (28)

$$G^{\alpha\beta} = \mu[(\mathbf{s}^{\beta *} S^{\beta\alpha}) \cdot \mathbf{m}^\alpha + \mathbf{s}^\alpha \cdot (\mathbf{s}^{\beta *} M^{\beta\alpha})] + \partial_A \hat{y}(A, \vartheta). \tag{30}$$

In the case of linearly dependent (redundant) constraints in $\mathscr{A}$, the matrix $\mathbf{G} := G^{\alpha\beta}$ defined in eqn (30) is singular and its inverse does not exist. Then the incremental slips are not uniquely determined. In order to handle this problem, we propose here a solution of the system (29) for the incremental slips with a *generalized inverse* as follows. Firstly, we perform a triangular factorization $\mathbf{G} = \mathbf{LDU}$. Next, we drop rows with zero diagonal elements and introduce the non-square matrix $\tilde{\mathbf{G}} := \tilde{G}^{\tilde{\alpha}\beta}$ and the modified residual matrix $\tilde{\boldsymbol{\phi}} := \tilde{\phi}^{\tilde{\alpha}}$ with $\tilde{\alpha} \in \tilde{\mathscr{A}} \subset \mathscr{A}$, where $\tilde{\mathscr{A}}$ is a reduced active set. Finally, we compute the generalized inverse associated with the reduced active set $\tilde{\mathbf{G}}^{-1} := \tilde{\mathbf{G}}^{\mathrm{T}}(\tilde{\mathbf{G}}\tilde{\mathbf{G}}^{\mathrm{T}})^{-1}$ and execute the Newton update (3.10) with the generalized inverse in the space of the reduced active set $\tilde{\mathscr{A}}$, i.e., $\gamma^\alpha \Leftarrow \gamma^\alpha + \Sigma_{\tilde{\beta} \in \tilde{\mathscr{A}}} \tilde{G}^{\alpha\tilde{\beta} -1} \tilde{\phi}^{\tilde{\beta}}$.

The active working set is now updated in each Newton iteration step by means of the following procedure. Firstly, the additional update

$$\gamma^\alpha \Leftarrow \max [0, \gamma^\alpha] \tag{31}$$

restricts the plastic parameters to strictly positive values during the iteration. Secondly, the *current active working* set is computed via

$$\mathscr{A} = \mathscr{A}^\phi \cup \mathscr{A}^\gamma \quad \text{with} \quad \begin{cases} \mathscr{A}^\phi := \{\alpha \in \mathscr{S} \mid \phi^\alpha > \mathrm{tol}_\phi\} \\ \mathscr{A}^\gamma := \{\alpha \in \mathscr{S} \mid \gamma^\alpha > 0\} \end{cases}. \tag{32}$$

Convergence of the iterative procedure with current change of the active set is obtained for

$$\mathscr{A}^\phi = \varnothing, \tag{33}$$

i.e., when consistency is restored for the current active set $\mathscr{A}$. Otherwise, the iteration sequence is repeated for the current active set starting with new Eulerian vector updates in eqn (26). The algorithm is summarized in Table 3.

3.3. *Exact volume-preserving postprocessing update*

As already mentioned above, we observe that the algorithm (21) does not in general preserve the volume of its tensor argument. Its output $\tilde{\mathbf{F}}^e$ is in general not a unimodular tensor, i.e., we have the situation $\tilde{J}^e := \det[\tilde{\mathbf{F}}^e] \neq 1$. We now propose an algorithm acting as a correcting postprocessor within each step of the overall global equilibrium iteration. This algorithm again exploits critically the assumed decoupled representation of the hyperelastic stress response into decoupled volumetric and isochoric contributions. The basic idea is to *scale the trace* of the elastic left Finger tensor $\tilde{\mathbf{b}}^e := \tilde{\mathbf{F}}^e \tilde{\mathbf{F}}^{e\mathrm{T}}$ such that $\det[\tilde{\mathbf{b}}^e] = 1$ holds exactly.

Table 3. Stress update for rate-independent monocrystal thermoplasticity

(*i*) *Elastic predictor*

$\{\mathbf{F}, \vartheta\}$ and $\{\tilde{\mathbf{F}}_n^{p-1}, A_n\}$ are given. Compute $J := \det[\mathbf{F}]$ and get trial values $\tilde{\mathbf{F}}^{e*} := J^{-1/3}\mathbf{F}\tilde{\mathbf{F}}_n^{p-1}$, $\mathbf{s}^{\alpha*} := \tilde{\mathbf{F}}^{e*}\mathbf{S}^\alpha$ and $\mathbf{m}^{\alpha*} := \tilde{\mathbf{F}}^{e*}\mathbf{M}^\alpha$. Evaluate for all $\alpha \in \mathscr{S}$

$$\phi^{\alpha*} = \mu \mathbf{s}^{\alpha*} \cdot \mathbf{m}^{\alpha*} - \hat{y}(A_n, \vartheta).$$

If $\phi^{\alpha*} \leqslant \text{tol}_\phi$ for all $\alpha \in \mathscr{S}$ set $\tilde{\mathbf{F}}^e = \tilde{\mathbf{F}}^{e*}$, $\tilde{\mathbf{F}}^{p-1} = \tilde{\mathbf{F}}_n^{p-1}$, $A = A_n$, $\mathscr{A} = \varnothing$ and go to (iv). Else first define estimate $\mathscr{A} = \{\alpha \in \mathscr{S} \mid \phi^{\alpha*} > \text{tol}_\phi\}$ for active working set.

(*ii*) *Return mapping in terms of Eulerian vectors*

(1) Set initial values $\gamma^\alpha = 0$ for all $\alpha \in \mathscr{S}$

(2) Compute for active systems $\alpha, \beta \in \mathscr{A}$

$$\mathbf{s}^\alpha = \mathbf{s}^{\alpha*} - \Sigma_{\beta \in \mathscr{A}} \gamma^\beta \mathbf{s}^{\beta*} S^{\beta\alpha}$$

$$\mathbf{m}^\alpha = \mathbf{m}^{\alpha*} - \Sigma_{\beta \in \mathscr{A}} \gamma^\beta \mathbf{s}^{\beta*} M^{\beta\alpha}$$

$$A = A_n + \Sigma_{\alpha \in \mathscr{A}} \gamma^\alpha$$

$$\phi^\alpha = \mu \mathbf{s}^\alpha \cdot \mathbf{m}^\alpha - \hat{y}(A, \vartheta)$$

$$G^{\alpha\beta} = \mu[(\mathbf{s}^{\beta*} S^{\beta\alpha}) \cdot \mathbf{m}^\alpha + \mathbf{s}^\alpha \cdot (\mathbf{s}^{\beta*} M^{\beta\alpha})] + \partial_A \hat{y}(A, \vartheta).$$

(3) Update plastic parameters $\gamma^\alpha \Leftarrow \gamma^\alpha + \Sigma_{\beta \in \mathscr{A}} G^{\alpha\beta - 1} \phi^\beta$ with generalized inverse.

(4) Perform active set update $\gamma^\alpha \Leftarrow \max[0, \gamma^\alpha]$.

(5) Set up $\mathscr{A}^\phi := \{\alpha \in \mathscr{S} \mid \phi^\alpha > \text{tol}_\phi\}$ and $\mathscr{A}^\gamma := \{\alpha \in \mathscr{S} \mid \gamma^\alpha > 0\}$.

(6) Redefine active working set $\mathscr{A} = \mathscr{A}^\phi \cup \mathscr{A}^\gamma$. If $(\mathscr{A}^\phi \neq \varnothing)$ go to 2.

(*iii*) *Update of intermediate configuration*

Compute isochoric elastic deformation gradient $\tilde{\mathbf{F}}^e = \tilde{\mathbf{F}}^{e*} - \Sigma_{\alpha=1}^m \gamma^\alpha \mathbf{s}^{\alpha*} \otimes \mathbf{M}^\alpha$, perform polar decomposition $\tilde{\mathbf{F}}^e = \tilde{\mathbf{b}}^{e1/2}\tilde{\mathbf{R}}^e$, compute scalar f from cubic equation $\det[\det[\tilde{\mathbf{b}}^e] + f\mathbf{1}] = 1$ and perform update $\tilde{\mathbf{F}}^{p-1} = \tilde{\mathbf{F}}^{-1}(\text{dev}[\tilde{\mathbf{b}}^e] + f\mathbf{1})^{1/2}\tilde{\mathbf{R}}^e$.

(*iv*) *Eulerian deviatoric stresses and moduli*

Compute Eulerian stresses and algorithmic moduli

$$\tau = p\mathbf{1} + \mu \,\text{dev}[\tilde{\mathbf{b}}^e] \quad \text{with} \quad p = \kappa \ln[J] - \kappa\delta(\vartheta - \vartheta_0)$$

$$c = (\kappa + p)\mathbf{1} \otimes \mathbf{1} - 2p\mathbb{I} + \tfrac{2}{3}\mu \,\text{tr}[\tilde{\boldsymbol{b}}^e][\mathbb{I} - \tfrac{1}{3}\mathbf{1} \otimes \mathbf{1}] - \tfrac{2}{3}[\text{dev}[\tau] \otimes \mathbf{1} + \mathbf{1} \otimes \text{dev}[\tau]]$$

$$- \Sigma_{\alpha \in \mathscr{A}} \Sigma_{\beta \in \mathscr{A}} G^{\alpha\beta - 1} \mu \,\text{dev}[\mathbf{s}^{\alpha*} \otimes \mathbf{m}^\alpha + \mathbf{m}^\alpha \otimes \mathbf{s}^{\alpha*}] \otimes \mu \,\text{dev}[\mathbf{s}^\beta \otimes \mathbf{m}^\beta + \mathbf{m}^\beta \otimes \mathbf{s}^\beta]$$

This modification does not influence the deviatoric stresses of the isotropic model under consideration, which are determined in terms of the deviator dev$[\tilde{\mathbf{b}}^e]$, and therefore keeps the Schmid stresses defined in eqn (18) untouched. As a consequence, the corrector update can be performed as a postprocessor of the return-mapping algorithm outlined in the subsection above.

Based on the polar decomposition $\tilde{\mathbf{F}}^e = \tilde{\mathbf{b}}^{e1/2}\tilde{\mathbf{R}}^e$ we consider the following corrector update:

$$\tilde{\mathbf{F}}^e \Leftarrow (\text{dev}[\tilde{\mathbf{b}}^e] + f\mathbf{1})^{1/2}\tilde{\mathbf{R}}^e, \tag{34}$$

where the scalar f is computed from the cubic equation

$$\det[\text{dev}[\tilde{\mathbf{b}}^e] + f\mathbf{1}] = 1. \tag{35}$$

This equation can be recast in the form

$$f^3 - J_2 f - (1 - J_3) = 0 \tag{36}$$

in terms of the two invariants

$$J_2 := \tfrac{1}{2}\text{dev}[\tilde{\mathbf{b}}^e] : \text{dev}[\tilde{\mathbf{b}}^e] \quad \text{and} \quad J_3 := \det[\text{dev}[\tilde{\mathbf{b}}^e]] \tag{37}$$

of the given deviator dev$[\tilde{\mathbf{b}}^e]$. Equation (36) is then solved via a Newton iteration based on the initial value $f = \frac{1}{3}\text{tr}[\tilde{\mathbf{b}}^e]$, giving the update

$$f \Leftarrow f - [f^3 - J_2 f - (1 - J_3)]/[3f^2 - J_2] \tag{38}$$

within each iteration. The iteration converges after a very few steps.

3.4. *Algorithmic Eulerian elastoplastic moduli*

In the Eulerian format, the Kirchhoff stresses of the model under consideration are given in terms of the decoupled spherical and deviatoric contributions

$$\boldsymbol{\tau} = p\mathbf{g}^{-1} + \boldsymbol{\tau}_{\text{iso}} \quad \text{with} \quad p = \kappa \ln[J] - \kappa\,\delta(\vartheta - \vartheta_0) \tag{39}$$

associated with the volumetric and isochoric part of the deformation. The deviatoric stresses take the form

$$\boldsymbol{\tau}_{\text{iso}} = \mu\,\text{dev}[\bar{\mathbf{b}}^{\text{e}}], \tag{40}$$

where the elastic Finger tensor $\bar{\mathbf{b}}^{\text{e}}$ is given by the algorithm

$$\bar{\mathbf{b}}^{\text{e}} = \bar{\mathbf{F}}^{\text{e}}\bar{\mathbf{F}}^{\text{eT}} \quad \text{with} \quad \bar{\mathbf{F}}^{\text{e}} = [\bar{\mathbf{F}}^{\text{e}*} - \sum_{\alpha \in \mathscr{A}} \gamma^{\alpha}\mathbf{s}^{\alpha *} \otimes \mathbf{M}^{\alpha}]. \tag{41}$$

The so-called algorithmic or consistent Eulerian elastoplastic moduli c govern the rate equation

$$\mathscr{L}_{\Delta}\boldsymbol{\tau} = c : \text{sym}[\nabla^{\Delta}\hat{\boldsymbol{\varphi}}] \quad \text{with} \quad c := 2\partial_{\mathbf{g}}\boldsymbol{\tau}(\mathbf{g}; \mathbf{F}^{\text{e}}, \vartheta). \tag{42}$$

Here $\mathscr{L}_{\Delta}\boldsymbol{\tau} := \Delta\boldsymbol{\tau} - \nabla^{\Delta}\hat{\boldsymbol{\varphi}}\boldsymbol{\tau} - \boldsymbol{\tau}\nabla^{\text{T}}\hat{\boldsymbol{\varphi}}^{\Delta}$ denotes the Oldroyd-type incremental stress rate and $\nabla^{\Delta}\hat{\boldsymbol{\varphi}} := (\Delta\mathbf{F})\mathbf{F}^{-1}$ is the spatial gradient of a vector field $\hat{\boldsymbol{\varphi}}^{\Delta}$ of incremental deformations defined on the current configuration. As pointed out in eqn $(42)_2$, the Eulerian moduli c are obtained as the derivative of the algorithmic expression for the Kirchhoff stresses in terms of the standard Eulerian metric $\mathbf{g}$.

We first derive the volumetric part of the moduli. With the standard results $\partial_{\mathbf{g}}J = \frac{1}{2}J\mathbf{g}^{-1}$ and $\partial_{\mathbf{g}}[\mathbf{g}^{-1}] = -\mathbb{I}_{\mathbf{g}^{-1}}$ we at once obtain

$$c^{\text{e}}_{\text{vol}} = 2\,\partial_{\mathbf{g}}[p\mathbf{g}^{-1}] = \kappa\mathbf{g}^{-1} \otimes \mathbf{g}^{-1} - 2p\mathbb{I}_{\mathbf{g}^{-1}}. \tag{43}$$

The isochoric part is given by the algorithmic expression (41) and is in particular a function of the active plastic slip increments γ^{α} for $\alpha \in \mathscr{A}$. Therefore, we consider the decomposition

$$c_{\text{iso}} = c^{\text{e}}_{\text{iso}} - c^{\text{p}}_{\text{iso}} \tag{44}$$

into an elastic part $c^{\text{e}}_{\text{iso}}$ and a plastic softening part $c^{\text{p}}_{\text{iso}}$. The elastic part is obtained by a fictitious freezing of the plastic slip. Recalling $\bar{\mathbf{F}}^{\text{e}} = J^{-1/3}\mathbf{F}^{\text{e}}$ and taking into account the dependence of the trace and deviator operators on the current metric, $\text{tr}[(\cdot)] := \mathbf{g} : (\cdot)$ and $\text{dev}[(\cdot)] := (\cdot) - \frac{1}{3}\text{tr}[(\cdot)]\mathbf{g}^{-1}$, one obtains the standard result

$$c^{\text{e}}_{\text{iso}} := 2\,\partial_{\mathbf{g}}\boldsymbol{\tau}_{\text{iso}} \,|_{\gamma^{\alpha}} = \tfrac{2}{3}\mu\,\text{tr}\,[\bar{\mathbf{b}}^{\text{e}}][\mathbb{I}_{\mathbf{g}^{-1}} - \tfrac{1}{3}\mathbf{g}^{-1} \otimes \mathbf{g}^{-1}] - \tfrac{2}{3}[\boldsymbol{\tau}_{\text{iso}} \otimes \mathbf{g}^{-1} + \mathbf{g}^{-1} \otimes \boldsymbol{\tau}_{\text{iso}}] \tag{45}$$

for the Neo-Hookean model under consideration. The plastic softening part is defined as

$$c^{\text{p}}_{\text{iso}} := -\Sigma_{\alpha \in \mathscr{A}}\,\partial_{\gamma^{\alpha}}\boldsymbol{\tau}_{\text{iso}} \otimes 2\,\partial_{\mathbf{g}}\gamma^{\alpha}. \tag{46}$$

Here, the first derivative, based on the algorithmic representation $(41)_2$, takes the simple form

$$-\partial_{\gamma^\alpha}\boldsymbol{\tau}_{\mathrm{iso}} = \mu\,\mathrm{dev}\,[\mathbf{s}^{\alpha *}\otimes\mathbf{m}^\alpha + \mathbf{m}^\alpha\otimes\mathbf{s}^{\alpha *}]. \tag{47}$$

The second derivative can be obtained via the implicit function theorem from the consistency condition $\phi^\alpha = \tau^\alpha - y = 0$ for $\alpha\in\mathscr{A}$ which yields with the definition $(29)_2$ the representation

$$2\,\partial_{\mathbf{g}}\gamma^\alpha = \Sigma_{\beta\in\mathscr{A}} G^{\alpha\beta\,-1}\,2\,\partial_{\mathbf{g}}\phi^\alpha\,|_{\gamma^\alpha}. \tag{48}$$

Based on the Eulerian representation of the Schmid stress for the model under consideration, $\tau^\alpha = \mu\mathbf{g}:[\mathbf{s}^\alpha\otimes\mathbf{m}^\alpha + \mathbf{m}^\alpha\otimes\mathbf{s}^\alpha]/2$ we conclude by taking into account the relationships (18)

$$2\,\partial_{\mathbf{g}}\phi^\alpha\,|_{\gamma^\alpha} = \mu\,\mathrm{dev}\,[\mathbf{s}^\alpha\otimes\mathbf{m}^\alpha + \mathbf{m}^\alpha\otimes\mathbf{s}^\alpha]. \tag{49}$$

Insertion of eqns (47)–(49) into eqn (46) then yields the final result

$$c^{\mathrm{p}}_{\mathrm{iso}} = \Sigma_{\alpha\in\mathscr{A}}\Sigma_{\beta\in\mathscr{A}} G^{\alpha\beta\,-1}\,\mu\,\mathrm{dev}\,[\mathbf{s}^{\alpha *}\otimes\mathbf{m}^\alpha + \mathbf{m}^\alpha\otimes\mathbf{s}^{\alpha *}]\otimes\mu\,\mathrm{dev}\,[\mathbf{s}^\beta\otimes\mathbf{m}^\beta + \mathbf{m}^\beta\otimes\mathbf{s}^\beta] \tag{50}$$

for the isochoric plastic softening part. The total Eulerian moduli are summarized in Table 3 and consist of the parts

$$c = c^{\mathrm{e}}_{\mathrm{vol}} + c^{\mathrm{e}}_{\mathrm{iso}} - c^{\mathrm{p}}_{\mathrm{iso}}. \tag{51}$$

Observe the extremely simple representation in terms of the Eulerian vectors $(\mathbf{s}^\alpha, \mathbf{m}^\alpha)$ of the slip systems $\alpha\in\mathscr{A}$. The moduli are in general unsymmetric. The case where only one slip system is active plays a particular role. Then $G^{\alpha\beta}$ reduces to a real number and we deduce from eqn (26) the specific result $\mathbf{s}^{\alpha *} = \mathbf{s}^\alpha$. Thus in this particular case the moduli are symmetric.

4. GLOBAL SOLUTION ALGORITHM AND FE-DISCRETIZATION

This section summarizes the initial-boundary-value problem of finite strain thermoplasticity, provides information about the applied global solution algorithm for the coupled thermomechanical problem and finally makes some remarks concerning the finite element discretization.

4.1. *Initial-boundary-value problem of coupled thermoplasticity*

The first central global equation of coupled thermoplasticity is the local form of the balance of linear momentum. In a Eulerian setting relative to the current configuration we get

$$\rho_0\dot{\mathbf{v}} = J\,\mathrm{div}\,[\boldsymbol{\tau}/J] + \boldsymbol{\gamma}, \tag{52}$$

where $\boldsymbol{\gamma}$ denotes a given body-force field and $\mathrm{div}[\cdot]$ is the spatial divergence operator with respect to the current coordinates $x = \varphi_t(X)$. The second essential global equation is the balance of internal energy

$$\dot{e} = \boldsymbol{\tau}:\mathbf{d} + J\,\mathrm{div}\,[-\mathbf{q}/J] + \mathscr{R}, \tag{53}$$

where $\mathbf{q}$ denotes the Kirchhoff heat-flux vector and $\mathscr{R}$ a given heat source with respect to the unit of the reference volume. $\boldsymbol{\tau}:\mathbf{d}$ with $\mathbf{d} := \mathrm{sym}[\mathbf{g}\nabla_x\mathbf{v}]$ is the stress power with respect to the unit of the reference volume. Based on the Legendre transformation $e = \psi + \vartheta\eta$, we obtain with the constitutive equations in Table 2 the evolution $\dot{e} = \boldsymbol{\tau}:\mathbf{d} + \vartheta\dot{\eta} - \mathscr{D}^{\mathrm{p}}$ and therefore, alternatively to eqn (53), an evolution equation

$$\vartheta\dot{\eta} = J\,\mathrm{div}\,[-\mathbf{q}/J] + \mathscr{R} + \mathscr{D}^{\mathrm{p}} \tag{54}$$

for the entropy. $\mathscr{D}^{\mathrm{p}} \geqslant 0$ is the plastic dissipation defined in eqn (19). By taking into account the constitutive rate equation $\vartheta\dot{\eta} = c\dot{\vartheta} - \mathscr{H}$ with the heat capacity and thermoelastic heating,

$$c := -\vartheta\,\partial^2_{\vartheta\vartheta}\hat{\psi} \quad \text{and} \quad \mathscr{H} := \vartheta\,\partial_{\vartheta}[\boldsymbol{\tau} : \mathbf{d} - \mathscr{D}^{\mathrm{p}}], \tag{55}$$

we end up with an evolution equation for the temperature

$$c\dot{\vartheta} = \{J\,\mathrm{div}\,[-\mathbf{q}/J] + \mathscr{R}\} + \{\mathscr{H} + \mathscr{D}^{\mathrm{p}}\}. \tag{56}$$

Note that the first bracket vanishes in an adiabatic process, i.e., for $\mathbf{q} \equiv 0$ and $\mathscr{R} \equiv 0$. Equation (55) is known as the coupled temperature evolution equation of thermoplasticity. The last two terms on the right-hand side characterize the thermoelastic and dissipative coupling effects. In applications of metal thermoplasticity we have the situation $|\mathscr{H}| \ll \mathscr{D}^{\mathrm{p}}$. In those applications one can neglect the thermoelastic heating effect by setting $\mathscr{H} \approx 0$.

The quantification of the plastic dissipation $\mathscr{D}^{\mathrm{p}}$ is a difficult task. We refer in this context to Taylor and Quinney (1933) and the review article Bever *et al.* (1973) with references therein. The constitutive model outlined above relates the dissipation, see expression (19), to the power associated with the initial flow stress while the hardening part is assumed to be completely stored in the material. This does not fit with experimental data on metal plasticity which indicate that in addition a part of the hardening power dissipates. In order to circumvent the necessary introduction of additional internal variables for the description of this phenomenon, we assume here that a certain fraction $\chi \in [0, 1]$ of the total plastic power, the first term in eqn (11), converts into heat. For the isotropic Taylor model outlined in Table 2 we get

$$\mathscr{D}^{\mathrm{p}} \approx \chi[\hat{\tau}_0(\vartheta) + \hat{B}(A, \vartheta)]\dot{A} \geqslant 0. \tag{57}$$

The initial-boundary-value problem of coupled thermoelasticity is completed by a constitutive equation for the heat flux. In this treatment, the flux in the interior of the body is assumed to be governed by an isotropic Eulerian Fourier law for the Kirchhoff heat flux

$$\mathbf{q} = -k\nabla\vartheta, \tag{58}$$

where $k > 0$ denotes the heat conductivity.

With regard to the construction of algorithms for the solution of the coupled problem, it makes sense to write the global field equations as a first-order evolution system

$$\left.\begin{aligned} \dot{\boldsymbol{\varphi}} &= \mathbf{v}, \\ \dot{\mathbf{v}} &= \frac{1}{\rho_0} J\,\mathrm{div}[\boldsymbol{\tau}/J], \\ \dot{\vartheta} &= \frac{1}{c} J\,\mathrm{div}\,[-\mathbf{q}/J] + \frac{1}{c}\mathscr{D}^{\mathrm{p}}, \end{aligned}\right\} \tag{59}$$

where we have dropped the given source terms γ, $\mathscr{R}$ and $\mathscr{H}$ in order to obtain a more compact representation. Taking into account the integration algorithms for the internal variables discussed in Section 3, we regard the right-hand side of eqn (59) as a function of the *primary variables* $\{\boldsymbol{\varphi}, \mathbf{v}, \vartheta\}$, the deformation field, the velocity field and the temperature field.

We now consider again a time interval $[t_n, t_{n+1}] \subset \mathbb{R}$ where the solution at time t_n is assumed to be known. Then the initial-boundary-value problem of coupled thermoplasticity is completed by the initial conditions

$$\{\boldsymbol{\varphi}, \mathbf{v}, \vartheta\}\,|_{(t=t_n)} = \{\varphi_n, \mathbf{v}_n, \vartheta_n\} \tag{60}$$

for the primary variables. The essential boundary conditions for the deformation field and the temperature field are

$$\boldsymbol{\varphi} = \bar{\boldsymbol{\varphi}} \quad \text{on} \quad \Gamma_\varphi \quad \text{and} \quad \vartheta = \bar{\vartheta} \quad \text{on} \quad \Gamma_\vartheta. \tag{61}$$

Finally, one has to take into account boundary conditions for the tractions $\mathbf{t}$ and the heat exchange q, i.e.,

$$\mathbf{t} := \boldsymbol{\tau} \cdot \mathbf{n} = \bar{\mathbf{t}} \quad \text{on} \quad \varphi(\Gamma_t) \quad \text{and} \quad q := \mathbf{q} \cdot \mathbf{n} = \bar{q} \quad \text{on} \quad \varphi(\Gamma_q) \tag{62}$$

with the decompositions of the surface of the reference configuration $\Gamma = \Gamma_\varphi \cup \Gamma_t = \Gamma_\vartheta \cup \Gamma_q$ and $\Gamma_\varphi \cap \Gamma_t = \varnothing$, $\Gamma_\vartheta \cap \Gamma_q = \varnothing$. The heat exchange is often assumed to be governed by a constitutive equation formulated in terms of the surface temperature of the form $\bar{q} = -k_c[\vartheta - \vartheta_\infty]$, where $k_c > 0$ is a convection coefficient and ϑ_∞ a given temperature of the surrounding medium.

4.2. *Thermomechanical coupling algorithm*

In the interval $[t_n, t_{n+1}]$ the system of thermomechanical equations (59) can be integrated. This results in a time-discrete system of equations which is fully coupled in the variables $\{\boldsymbol{\varphi}_{n+1}, \mathbf{v}_{n+1}, \vartheta_{n+1}\}$ at time t_{n+1}. Algorithms for such a monolithic set of non-linear coupled thermomechanical equations have been discussed for example by Argyris and Doltsinis (1981) and Simó and Miehe (1992), among others. In contrast to this approach, we consider here a scheme which yields an algorithmic decoupling within the time interval and results in partitioned symmetric structures for mechanical and thermal sub-problems. We base the construction of this algorithm on the methodology of operator-splitting which has recently been applied to coupled thermomechanical problems by Simó and Miehe (1992), Armero and Simó (1992), and Miehe (1993). The algorithm is obtained by a split of the non-linear evolution system (59) into the two parts

$$(M): \begin{cases} \dot{\boldsymbol{\varphi}} = \mathbf{v} \\ 0 = J \operatorname{div}[\boldsymbol{\tau}/J] \\ \dot{\vartheta} = 0 \end{cases} \quad \text{and} \quad (T): \begin{cases} \dot{\boldsymbol{\varphi}} = 0 \\ \dot{\mathbf{v}} = 0 \\ \dot{\vartheta} = \dfrac{1}{c} J \operatorname{div}[-\mathbf{q}/J] + \dfrac{1}{c}\mathscr{D}^p \end{cases} \tag{63}$$

for the quasistatic case. Problem (M) defines an isothermal sub-problem at *frozen temperature* ϑ_n which can be solved for the configuration $\boldsymbol{\varphi}$ and the velocity $\mathbf{v}$. Problem (T) is a pure thermal heat-conduction problem at *frozen configuration* φ which can be solved for the temperature ϑ. A sub-algorithm within the time step $\Delta t := t_{n+1} - t_n$ for the *isothermal deformation predictor* (M) based on a backward Euler integrator is governed by the equation

$$\hat{G}_M(\overset{*}{\boldsymbol{\varphi}}, \boldsymbol{\varphi}) := \int_{\mathscr{B}} \nabla \overset{*}{\boldsymbol{\varphi}} : \hat{\boldsymbol{\tau}}_{\text{algo}}(\boldsymbol{\varphi}; \vartheta_n)\, \mathrm{d}V - \int_{\boldsymbol{\varphi}(\Gamma_t)} \overset{*}{\boldsymbol{\varphi}} \cdot \bar{\mathbf{t}}\, \mathrm{d}a = 0 \tag{64}$$

and the update of the velocity $\mathbf{v} = (\boldsymbol{\varphi} - \boldsymbol{\varphi}_n)/\Delta t$. All variables without subscripts are understood to be evaluated at time t_{n+1}. The Eulerian stresses $\boldsymbol{\tau}_{\text{algo}}$ are obtained by executing the local stress update algorithm summarized in Table 3 at frozen temperature ϑ_n. The weak form (64) is obtained from the time-discrete counterpart of eqn $(63)_2$ by a standard Galerkin procedure along with the stress boundary condition $(62)_1$. $\overset{*}{\boldsymbol{\varphi}}$ is a virtual displacement field defined on the current configuration $\boldsymbol{\varphi}(\mathscr{B})$ which satisfies the homogeneous mechanical boundary conditions $\overset{*}{\boldsymbol{\varphi}} = 0$ on $\boldsymbol{\varphi}(\Gamma_\varphi)$. A sub-algorithm associated with the *heat conduction corrector* (T), again based on the backward Euler integrator, can be summarized by the weak form

$$\hat{G}_{\mathrm{T}}(\overset{*}{\vartheta}, \vartheta) := \int_{\mathscr{B}} \{\overset{*}{\vartheta} \frac{c}{\Delta t}(\vartheta - \vartheta_n) + \nabla \overset{*}{\vartheta} \cdot k \nabla \vartheta - \overset{*}{\vartheta} \mathscr{D}^{\mathrm{p}}_{\mathrm{algo}}\} \, \mathrm{d}V + \int_{\varphi(\Gamma_q)} \overset{*}{\vartheta} \bar{q} \, \mathrm{d}a = 0 \tag{65}$$

which follows in a standard Galerkin procedure from the time-discrete counterpart of $(63)_6$ by taking into account eqns (58) and $(62)_2$. In line with eqn (57), the algorithmic expression for the plastic dissipation is assumed to have the form $\mathscr{D}^{\mathrm{p}}_{\mathrm{algo}} \approx \chi \, [\hat{\tau}_0(\vartheta_n) + \hat{B}(A, \vartheta_n)] \, (A - A_n)/\Delta t$. It is considered as an output of the stress update algorithm in Table 3 which has already been performed in the isothermal predictor phase. $\overset{*}{\vartheta}$ denotes a virtual temperature field defined on the current configuration $\varphi(\mathscr{B})$ which satisfies the homogeneous thermal boundary conditions $\overset{*}{\vartheta} = 0$ on $\varphi(\Gamma_\vartheta)$. The overall thermomechanical coupling algorithm in a typical time step can be understood as a composition of the two subalgorithms (64) and (65).

4.3. *Algorithmic linearization*

With regard to the application of Newton-type solvers we now discuss the linearization of the two subproblems (M) and (T) outlined above. In order to obtain the linearization of the isothermal deformation predictor eqn (64) we write the linear increment of the Kirchhoff stresses at frozen temperature ϑ_n in the form $\Delta \boldsymbol{\tau}_{\mathrm{algo}} = c_{\mathrm{algo}} : \nabla \overset{\Delta}{\boldsymbol{\varphi}} + \nabla \overset{\Delta}{\boldsymbol{\varphi}} \, \boldsymbol{\tau}_{\mathrm{algo}} + \boldsymbol{\tau}_{\mathrm{algo}} \nabla^{\mathrm{T}} \overset{\Delta}{\boldsymbol{\varphi}}$. Here $\boldsymbol{\tau}_{\mathrm{algo}}$ and c_{algo} denote the algorithmic expressions for the Eulerian Kirchhoff stresses and moduli obtained from Table 3 at frozen temperature ϑ_n. Recall that $\nabla \overset{\Delta}{\boldsymbol{\varphi}}$ denotes the spatial gradient of an incremental displacement field $\overset{\Delta}{\boldsymbol{\varphi}}$ defined on the current configuration. Taking into account the increment $\Delta(\nabla \overset{*}{\boldsymbol{\varphi}}) = -\nabla \overset{*}{\boldsymbol{\varphi}} \nabla \overset{\Delta}{\boldsymbol{\varphi}}$ we obtain the linear increment of the weak form eqn (64)

$$\Delta \hat{G}_M(\overset{*}{\boldsymbol{\varphi}}, \overset{\Delta}{\boldsymbol{\varphi}}, \boldsymbol{\varphi}) := \int_{\mathscr{B}} \{\nabla \overset{*}{\boldsymbol{\varphi}} : \nabla \overset{\Delta}{\boldsymbol{\varphi}} \hat{\boldsymbol{\tau}}_{\mathrm{algo}}(\boldsymbol{\varphi}; \vartheta_n) + \nabla \overset{*}{\boldsymbol{\varphi}} : \hat{c}_{\mathrm{algo}}(\boldsymbol{\varphi}; \vartheta_n) : \nabla \overset{\Delta}{\boldsymbol{\varphi}}\} \, \mathrm{d}V, \tag{66}$$

in a straightforward manner characterized by the standard geometrical stress term and the material tangent term. Secondly, we compute the linearization of the heat-conduction corrector (65)

$$\Delta \hat{G}_T(\overset{*}{\vartheta}, \overset{\Delta}{\vartheta}, \vartheta) := \int_{\mathscr{B}} \{\overset{*}{\vartheta} \frac{c}{\Delta t} \overset{\Delta}{\vartheta} + \nabla \overset{*}{\vartheta} \cdot k \nabla \overset{\Delta}{\vartheta}\} \, \mathrm{d}V \tag{67}$$

for constant heat capacity c and conductivity k.

4.4. *Remarks on the finite element discretization*

The standard finite element approach introduces interpolations for the actual, virtual and incremental deformation fields $\{\varphi^{\mathrm{h}}, \overset{*}{\varphi}{}^{\mathrm{h}}, \overset{\Delta}{\varphi}{}^{\mathrm{h}}\}$ in eqn (64) and (66) and the actual, virtual and incremental temperature fields $\{\vartheta^{\mathrm{h}}, \overset{*}{\vartheta}{}^{\mathrm{h}}, \overset{\Delta}{\vartheta}{}^{\mathrm{h}}\}$ in eqns (65) and (67) in terms of discrete nodal temperatures. The discretizations of the variational formulations (64)–(67) yield the mechanical and thermal element residuals and element tangent matrices which are assembled in a typical Newton iteration step to form a global linear algebraic system for the mechanical and the thermal subproblem, respectively. For both the mechanical as well as the thermal field we assume identical finite element meshes which makes the transfer of coupling variables easy.

The standard displacement finite element approach fails in the context of isochoric elastoplasticity due to the overconstrained pressure field. To circumvent these difficulties, several mixed finite element formulations have been proposed in the literature. We discretize the mechanical phase of the algorithmically decoupled staggered scheme outlined above with mean pressure-dilatation four-node Q1P0 elements, see Simó and Miehe (1992) and references therein, or alternatively with incompatible-mode four-node Q1E4 elements developed by Simó and Armero (1992). A comparison of these different elements has been

Table 4. Material parameters

Bulk modulus	κ	49.980	kN mm^{-2}
Shear modulus	μ	21.100	kN mm^{-2}
Flow stress	y_0	0.0600	kN mm^{-2}
Saturation stress	$y_{0,\infty}$	0.0480	kN mm^{-2}
Saturation parameter	A_0	0.0929	—
Linear hardening	h	0.0010	kN mm^{-2}
Flow stress softening	ω	0.0020	K^{-1}
Expansion coefficient	δ	10^{-5}	K^{-1}
Heat conductivity	k	0.045	kN s^{-1} K^{-1}
Heat capacity	c	$3.558 \cdot 10^{-3}$	kN mm^{-2} K^{-1}
Dissipation factor	χ	0.9	—

made in the context of large-strain elasticity in Miehe (1994a), see also the references therein. The thermal phase can be discretized with standard displacement-type elements.

5. NUMERICAL EXAMPLES

The formulation described above has been implemented in an extended version of the general-purpose finite element program FEAP, developed by R. L. Taylor and J. C. Simó and partly documented in Chapter 24 of Zienkiewicz and Taylor (1989). The objective of this section is to assess the performance of the formulation and the constitutive integration algorithm discussed above for two typical examples of finite strain single-crystal thermoplasticity. For this purpose we choose for the constitutive model outlined in Table 2 the material parameters listed in Table 4, assumed to be valid for a given reference temperature $\vartheta_0 = 293$ K. They are suitable for a qualitative simulation of single crystal thermoplasticity. The isotropic Taylor hardening outlined in Table 2 is described by the initial flow stress function

$$\hat{\tau}_0(\vartheta) = y_0\{1-\omega(\vartheta-\vartheta_0)\} \tag{68}$$

and the saturation hardening function

$$\hat{B}(A,\vartheta) = \{y_{0,\infty}[1-\exp(-A/A_0)]+hA\}\{1-\omega(\vartheta-\vartheta_0)\} \tag{69}$$

in terms of the internal strain-like isotropic hardening variable A and the absolute temperature ϑ, see also the diagram in Fig. 3. The model can be easily extended to non-isotropic hardening effects which describe the well known overshooting phenomena in crystal plasticity, see for example Perzyna (1988) and Cutiño and Ortiz (1992) for a review.

The computations presented here are restricted to plane deformations under plane strain conditions. Furthermore, we restrict our investigations to *plane slip models*. Three possible plane slip arrangements are depicted in Fig. 2. The first one represents a *single slip system* with initial orientation θ_0 with respect to the X^1-axis of the Cartesian coordinate system at a material point of the isoclinic intermediate configuration. Observe that our notation distinguishes the slip directions by introducing two pairs of vectors $(\mathbf{S}^1, \mathbf{M}^1)$ and $(\mathbf{S}^2, \mathbf{M}^2)$ with $\mathbf{S}^2 = -\mathbf{S}^1$ and $\mathbf{M}^2 = \mathbf{M}^1$ for each slip system. Fig. 2(b) shows a *double slip arrangement* and Fig. 2(c) an *equilateral triangle model*, both initially orientated with the angle θ_0 relative to the X^1-axis. The latter is motivated by the closest package of cylinders with axis perpendicular to the plane of investigation, see, e.g., Harren and Asaro (1993). In the two examples below we apply exclusively the double slip arrangement depicted in Fig. 2(b). This planar double slip model has been suggested by Asaro (1979) based on experiments documented in Chang and Asaro (1981), and has since then been used in many rate dependent simulations of plane deformations of single crystals, see for example Peirce *et al.* (1982), Asaro and Needleman (1985) and Rashid and Nemat-Nasser (1992). In this model, the plastic deformation occurs by shearing on a pair of associated slip directions. The two individual slip systems maintain a fixed orientation β relative to each other, although the pair may rotate with respect to the Cartesian frame of the isoclinic intermediate

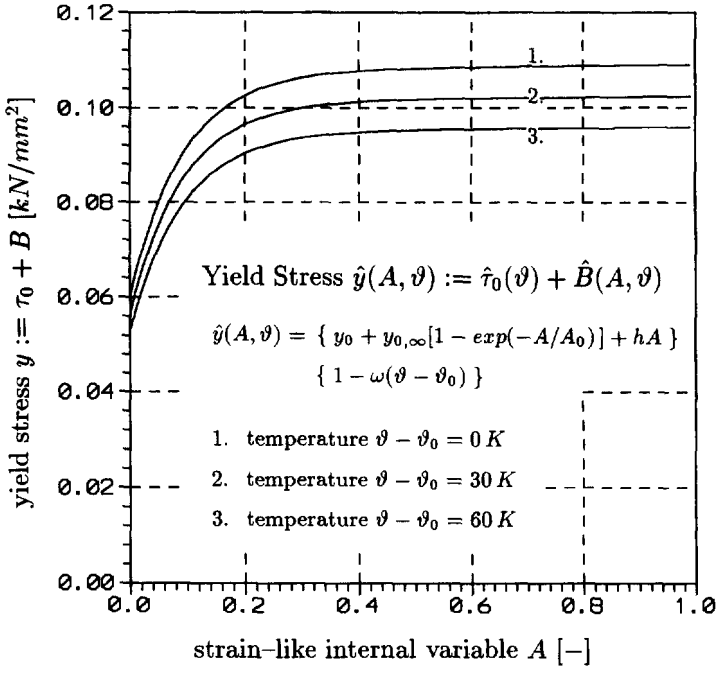

Fig. 3. Isotropic yield stress. Assumed dependence on internal strain-like variable A and relative temperature $\vartheta - \vartheta_0$.

configuration. The model can be applied to face-centred cubic (f.c.c.) metals such as aluminium and copper, which are known to flow on the closed packed {111} planes in the closest-packed [110] directions. For planar deformations in a {110} plane, the motion can be represented by a pair of *effective slip systems*.

All computations were performed on an IBM RISC 6000-340 workstation under the UNIX operating system.

5.1. *Homogeneous simple shear*

The first example shows the performance of the proposed algorithmic setting of rate-independent crystal plasticity for an isothermal homogeneous simple shear test. A similar problem has been numerically investigated for the rate-dependent case by Steinmann and Stein (1996). The initial geometry of this simple plane problem is depicted in Fig. 4(a),

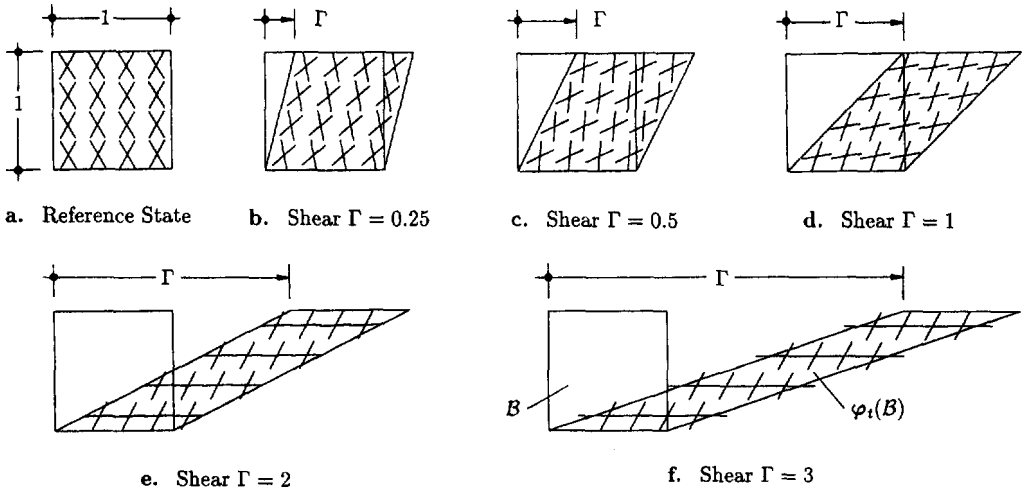

Fig. 4. Homogeneous simple shear. Rotation of the planar double slip arrangement (initial orientation $\theta = 60°$) for different global values Γ of simple shear. The relative orientation $\beta = 60°$ of the two slip planes remains constant.

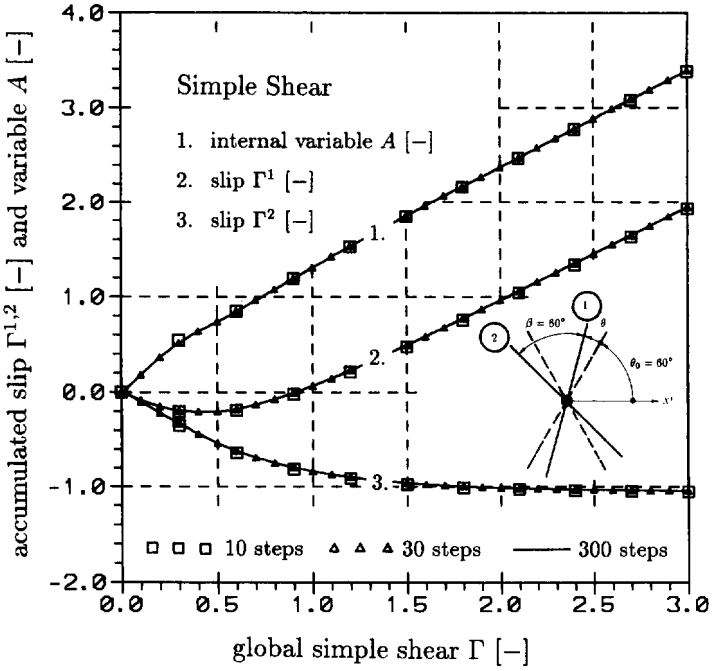

Fig. 5. Homogeneous simple shear. Accumulation of plastic slip Γ^1 and Γ^2 on the two slip systems 1 and 2 of the planar double slip arrangement. Evolution of the internal variable A.

characterized by the relation width/height = 1/1 mm. We apply the double slip arrangement described above and visualized in Fig. 2(b). The relative orientation has been chosen as $\beta = 60°$. Initial orientation is $\theta_0 = 60°$, i.e. the two slip planes are arranged at 30° symmetrically to the X^2-axis. The homogeneous problem has been discretized with 16 four-node finite elements. Figure 4(a) shows the initial orientation of the two slip planes at 16 material points, the centers of the elements, in the reference configuration $\mathscr{B}$. The successive shear deformation of the specimen is plotted in Fig. 4(b–f) for different values of global shear up to the value $\Gamma = 3[-]$. This sequence illustrates the elastoplastic response of the monocrystal under idealized plane conditions and points out in particular the successive lattice rotation of the slip arrangement.

The accumulated slip Γ^1 and Γ^2 on the two slip systems 1 (directions $\mathbf{S}^1$ and $\mathbf{S}^2$) and 2 (directions $\mathbf{S}^3$ and $\mathbf{S}^4$) as well as the evolution of the internal strain-like hardening variable A is documented in Fig. 5. The diagram in Fig. 6 shows the evolution of the lattice rotation θ of the double slip arrangement.

Let us turn our attention to the rotation of the double slip arrangement which is visualized in the plot sequence Fig. 4(b–f). As shown in diagram 6, the rate of rotation has its highest value at the beginning of the shearing process. For increasing amount Γ of global simple shear, the rotation converges towards the value $\vartheta_{\Gamma=3} \approx -60°$. Then, as shown in Fig. 4(e, f), slip system 1 is aligned to the X^1-axis. The diagram in Fig. 5 illustrates the plastic process on the two slip systems of the double slip arrangement. In the first stage of the process, the main slip occurs on system 2. System 1 sticks between the values $\Gamma \approx 0.40 - 0.50[-]$ of global shear, while system 2 is then roughly aligned to the X^2-axis. When the process of simple shear proceeds, system 1 becomes active again—with different sign—and now takes over the main slip, while the slip rate on system 2 converges towards zero. At high values of global shear Γ, system 1 is the only slip mechanism.

Clearly, these changes in the slip activity influence the Kirchhoff stress response. This is documented in Figs 7–9. Figure 7 depicts the shear stress τ_{12}. One observes considerable changes in the range $\Gamma = 0.4$–$0.5[-]$ of global shear, where system 1 first sticks and then becomes active again. Within this range the shear stress passes a limit point. Similar behaviour is observed for the normal stresses τ_{11} and τ_{22} depicted in Figs 8 and 9.

In order to investigate the accuracy performance of the proposed integration algorithm in Table 3, different time discretizations of the simple shear problem have been considered.

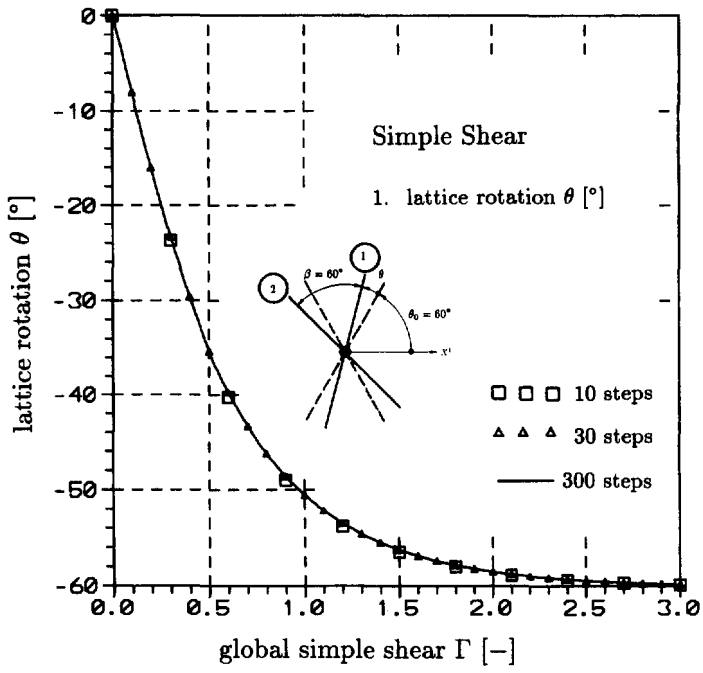

Fig. 6. Homogeneous simple shear. Rotation of the planar double slip arrangement.

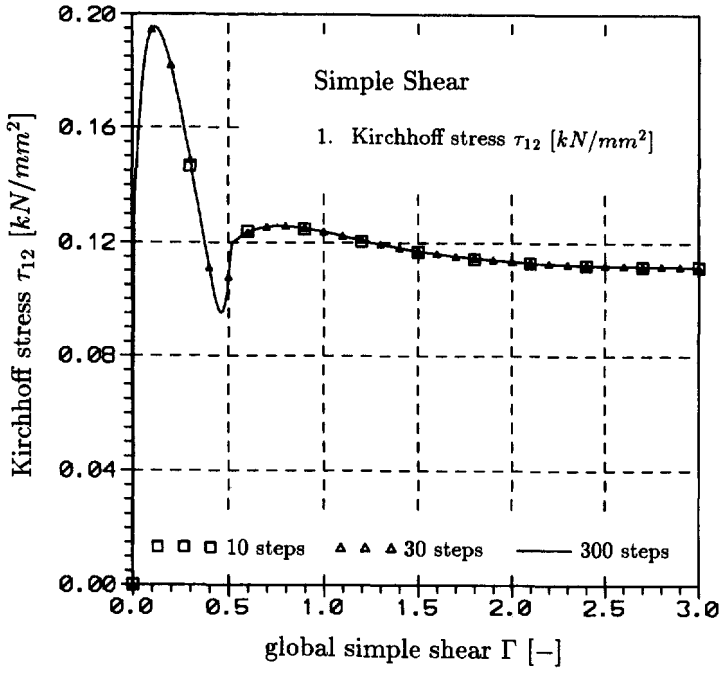

Fig. 7. Homogeneous simple shear. Evolution of Kirchhoff stress τ_{12}.

The final value $\Gamma = 3[-]$ has been obtained within 10, 30 and 300 equal steps. The results are documented and compared in the diagrams 5–9. It can be seen that, in the deformation controlled test under consideration, the plastic slip, the lattice rotation and the shear stress are almost independent of the step size. A considerable difference is observed only in the normal stress response τ_{11} and τ_{22} depicted in Figs 8 and 9. Here, sufficient accuracy needs a time discretization of at least 200 steps. In the author's opinion, this does not seem too much for the extreme large deformation of the model problem under consideration.

In the 300-step computation, the integration algorithm converges within an average of five steps.

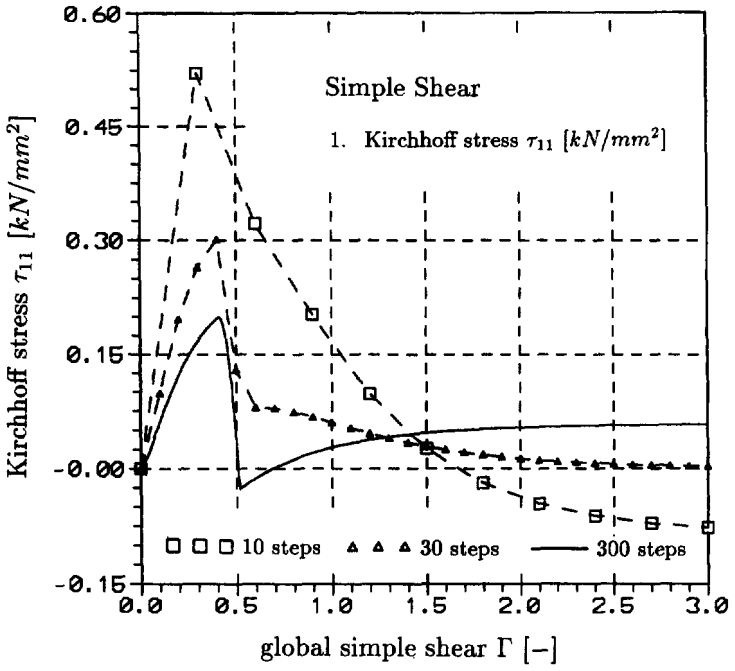

Fig. 8. Homogeneous simple shear. Evolution of Kirchhoff stress τ_{11}.

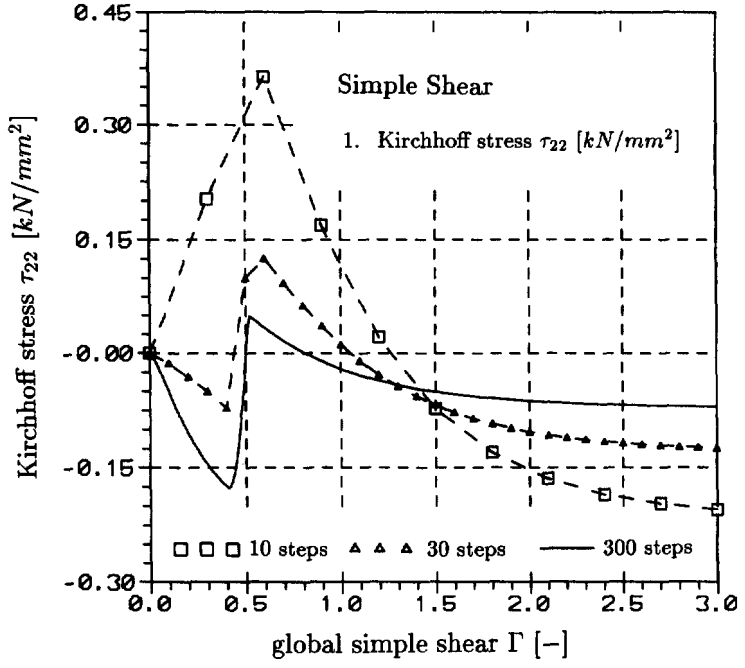

Fig. 9. Homogeneous simple shear. Evolution of Kirchhoff stress τ_{22}.

5.2. *Thermomechanical localization of a rectangular strip in tension*

We now consider the localization of a rectangular strip under plane strain conditions. Experimental foundations for this problem are reported in Chang and Asaro (1981), Spitzig (1981) and Duszek-Perzyna and Perzyna (1993). Numerical investigations are documented in Peirce *et al.* (1982, 1983), Needleman *et al.* (1985) and Rashid and Nemat-Nasser (1992) within a rate-dependent isothermal formulation. Here we treat the problem within the framework of rate-independent single crystal plasticity under non-isothermal quasi-static

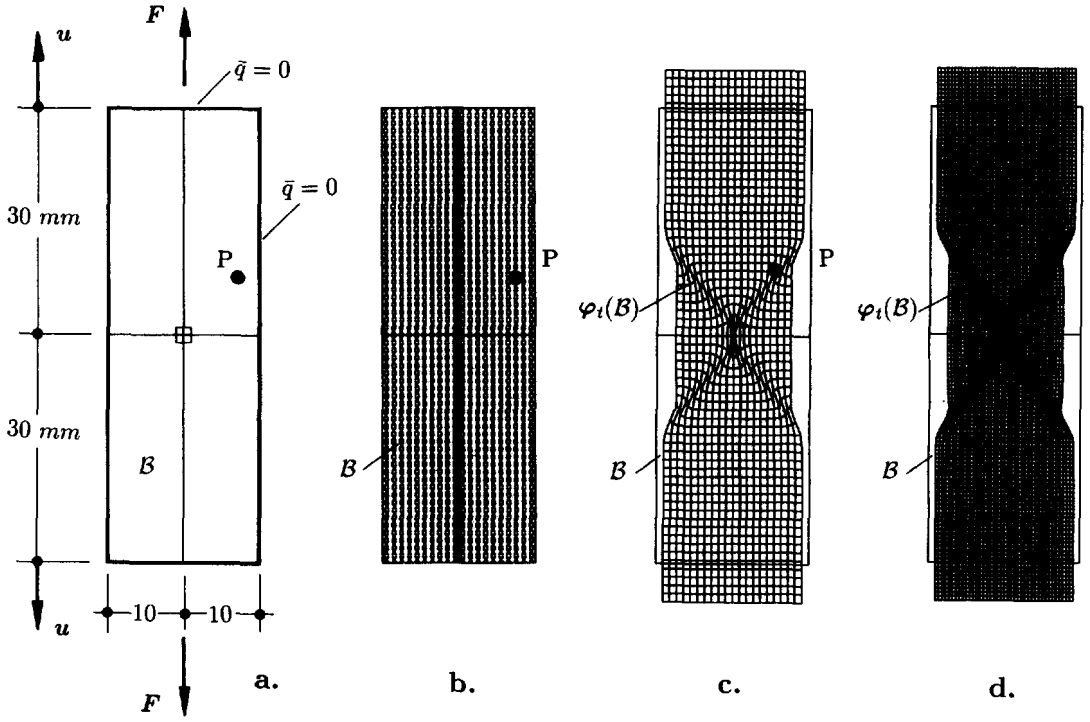

Fig. 10. Localization of a rectangular strip. (a) Geometry, mechanical and thermal boundary conditions, (b) homogeneous planar double slip arrangement in initial configuration, deformed mesh with (c) 4×300 elements and (d) 4×1200 elements at $u = 5$ mm and $\dot{u} = 10^4$ mm s^{-1}.

conditions. The geometry of the strip is depicted in Fig. 10(a) and is characterized by the relation width/length = 20/60 mm. The material parameters are identical with those of the previous example and summarized in Table 4. In order to trigger the localization of the geometrically perfect specimen we assume a material imperfection in the center of the specimen, as indicated by the square in Fig. 10(a). Here the flow stress values in Table 4 have been reduced by the factor 0.9. The prescribed mechanical boundary conditions at the two ends of the bar allow free contraction of the specimen.

As in the previous example we assume a double slip arrangement, see Fig. 2(b), with initial orientation $\theta_0 = 60^\circ$ and relative orientation $\beta_0 = 60^\circ$. Figure 10(b) depicts the homogeneous plane slip arrangement in the initial configuration $\mathcal{B}$.

In a displacement-controlled numerical test we deform the specimen up to a prescribed elongation $u = 5$ mm at both ends at a relatively high rate $\dot{u} = 10^4$ mm s^{-1}. At that speed the thermomechanical behaviour is almost adiabatic. As a consequence, we neglect the heat exchange on the surfaces of the specimen by assuming adiabatic thermal boundary conditions $\bar{q} = 0$. In the author's experience, the thermal boundary conditions for the geometrically imperfect specimen under consideration do not crucially influence the overall thermomechanical behaviour. The situation changes if one considers geometrically perfect specimens with initially homogeneous isothermal fields, where the thermal fields act as an imperfection on the mechanical fields. In this context we refer to the studies by Simó and Miehe (1992) and Armero and Simó (1992), where the triggering of localized deformation by the temperature field has been investigated.

By exploiting the symmetry of the problem only a quarter of the specimen has been discretized by 300 and 1200 four-node elements, respectively. Here the Q1/E4 enhanced incompatible mode element formulation mentioned in Section 4.4 with bilinear compatible and quadratic incompatible interpolations has been applied. These elements have proved to be very successful for the modelling of shear bands in localization analysis due to their good performance in bending dominated problems, see Simó and Armero (1992) and Armero and Simó (1992). Fig. 10(c, d) shows the deformed meshes with 4×300 and 4×1200 elements, respectively, at the final stage $u = 5$ mm where two crossed shear bands with an angle of ≈ 38.5 degrees with respect to the axis of the strip have been fully developed.

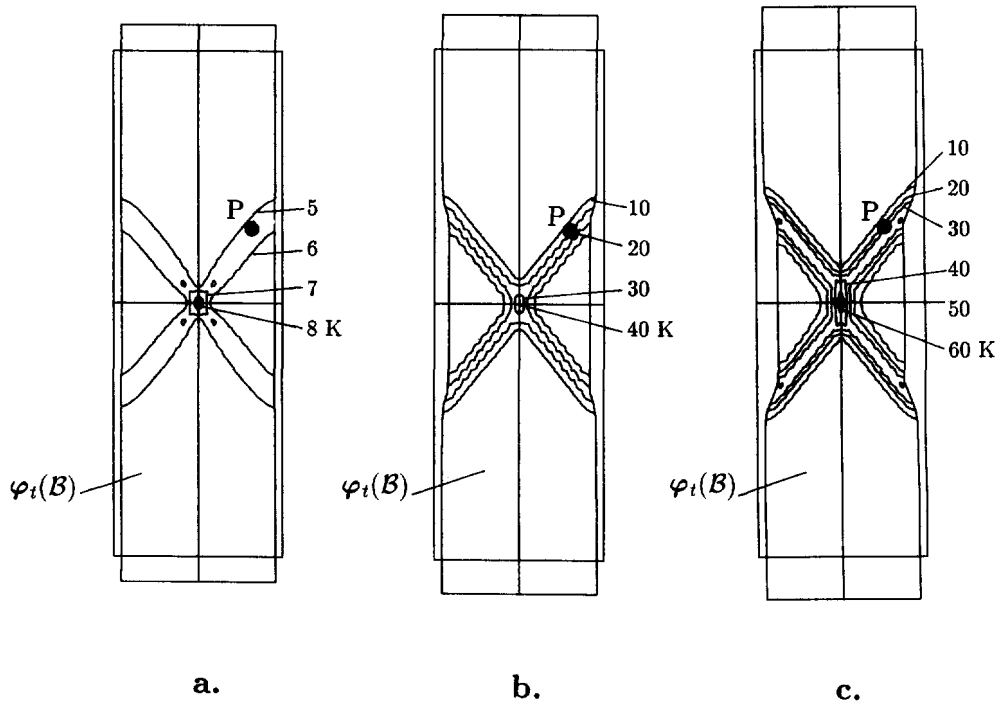

Fig. 11. Localization of a rectangular slip. Temperature distribution $\vartheta - \vartheta_0$ for (a) $u = 3$ mm, (b) $u = 4$ mm and (c) $u = 5$ mm at $\dot{u} = 10^4$ mm s^{-1}.

The elongation of the specimen was obtained in 30 equal time steps up to $u = 3.0$ mm followed by 200 equal time steps up to the final value $u = 5.0$ mm. In each time increment, the staggered global scheme discussed in Sections 4.2 and 4.3 has been applied. Here the nonlinear isothermal predictor (M) needed on average 5 Newton iterations based on the local constitutive algorithm outlined in Table 4. The heat conduction corrector (T) is linear due to the assumed temperature-independent thermal material parameters and therefore gives the solution within one step.

Figure 11(a–c) depicts the plastic zone and temperature distributions for the elongations $u = 3.0, 4.0, 5.0$ mm. In Fig. 12(a–c) we have plotted the rotation of the slip system 1. Inside the shear band, e.g., at the point P marked in Fig. 12, we observe a rotation of the slip direction from the initial value $\theta_0 = 60°$ to the final value $\theta_{u=5} = 51.5°$. It is evident that the slip systems reorient themselves within the shear band so that one slip plane may provide a mechanism of easy glide. We observe a reorientation of the slip systems in the area of the shear bands. In the positive quadrant, the lattice rotates as much as 8.5° clockwise, providing a mechanism of easy glide along the system 1.

Figure 13 depicts the load deflection curves associated with the two elongation rates and compares the mesh sensitivity. The computed maximum load is indicated by an L in the diagram. In the presence of the very fast—almost adiabatic—process one observes the well-known mesh dependence in the postcritical range. The diagrams in Figs 14–16 document state variables at the material point P of the specimen which is also indicated in the plots Figs 10–12. The onset of the localized shear band development is indicated by a bifurcation of the load deflection curve in Fig. 13 and the temperature evolution inside the shear band depicted in Fig. 14. This bifurcation appears shortly after the elongation $u = 3$ mm. Diagram 15 shows the same effect for the accumulated plastic slip Γ^1 and Γ^2 on the two systems 1 and 2 and the internal hardening variable A.

Almost immediately after the onset of the localization, the load drops as shown in Fig. 13. As already discussed in Asaro (1979) and Rashid and Nemat-Nasser (1992), this load drop is associated with the rather abrupt rotation of the crystal lattice in the shear band in the geometrically softer orientation. Figure 16 depicts the rotation of the lattice at the point

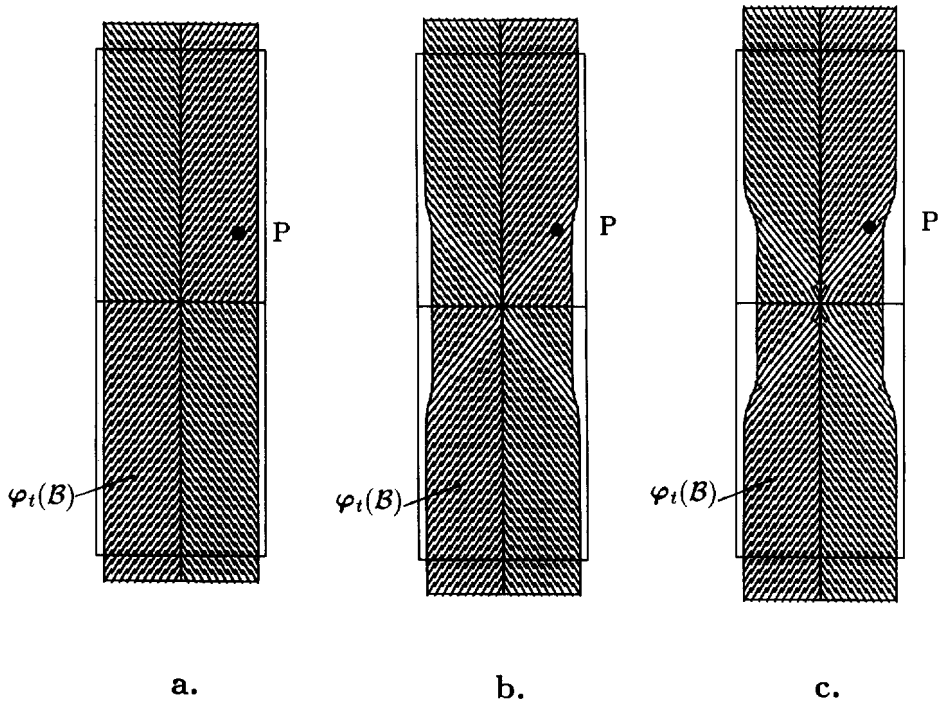

Fig. 12. Localization of a rectangular strip. Rotation of the slip system 1 for (a) $u = 3$ mm, (b) $u = 4$ mm and (c) $u = 5$ mm at $\dot{u} = 10^4$ mm s^{-1}.

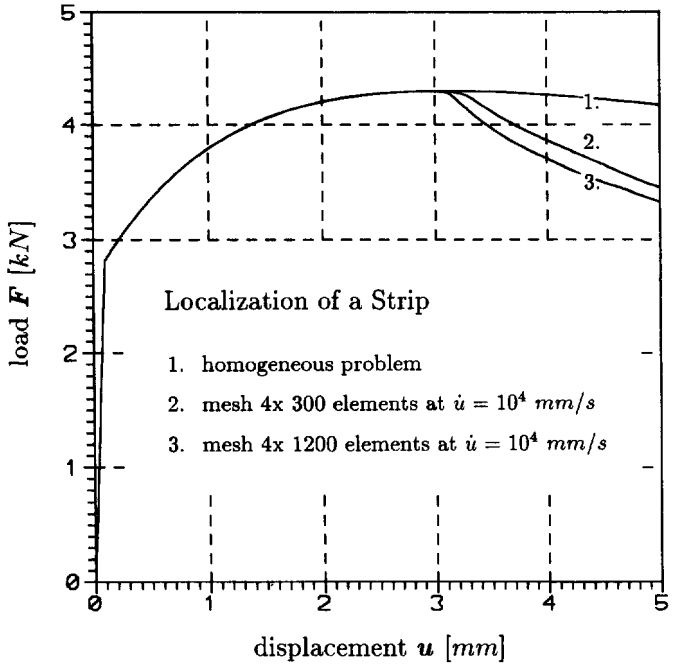

Fig. 13. Localization of a rectangular strip. Load deflection curves for two different meshes with 4×300 and 4×1200 elements at $\dot{u} = 10^4$ mm s^{-1}.

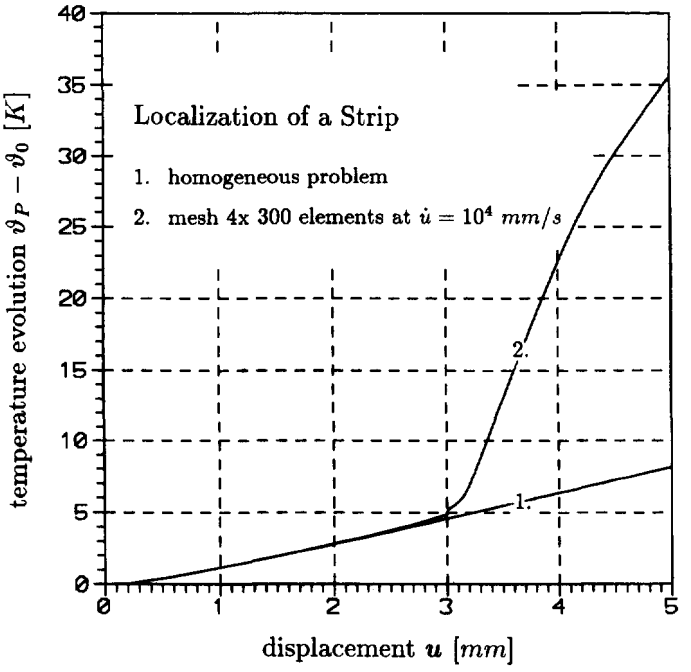

Fig. 14. Localization of a rectangular strip. Temperature evolution $\vartheta - \vartheta_0$ at the point P for homogeneous and inhomogeneous problems at $\dot{u} = 10^4$ mm s^{-1}.

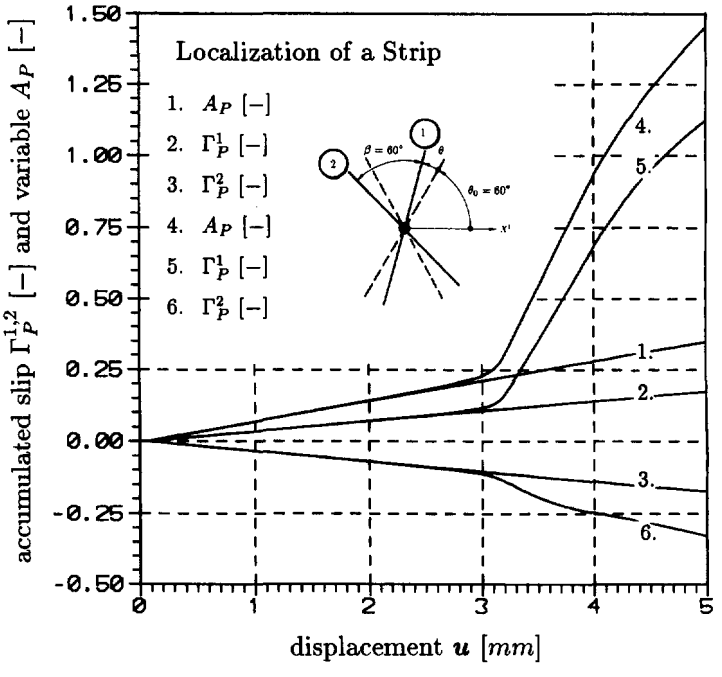

Fig. 15. Localization of a rectangular strip. Accumulation of plastic slip Γ^1 and Γ^2 on the two slip systems 1 and 2 of the planar double slip arrangement in the material point P. Evolution of the internal variable A in the point P.

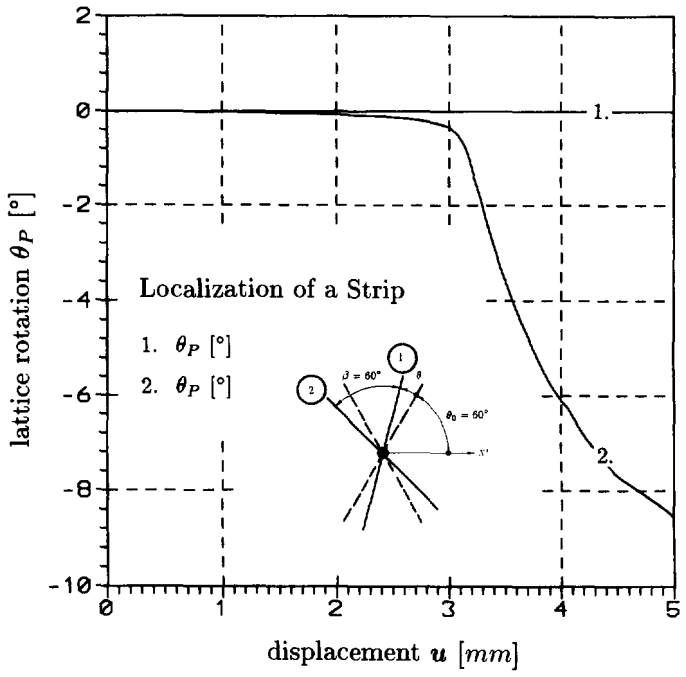

Fig. 16. Localization of a rectangular strip. Rotation of the planar double slip arrangement in the material point P.

P. The computation yields the final value $\theta_{u=5} \approx -8.5°$, which is also documented in the plot Fig. 12(c).

6. CONCLUSION

A formulation of rate-independent multisurface thermoplasticity for large-strain deformations of single crystals has been discussed with the emphasis on its numerical implementation. The underlying theoretical concept is the framework of multiplicative elastoplasticity which has been represented here in an intrinsic mixed-variant format. As a particular feature it turned out that the application of a Neo-Hookean-type model for the isochoric part of the elastic deformation results in a very convenient representation of the resolved shear stress which governs the plastic slip on a particular slip system. This observation has been intrinsically exploited within the algorithmic setting where the update algorithm for the plastic state variables could be represented in terms of simple updates of the Eulerian vectors aligned to active slip systems. In this new algorithmic setting, the multisurface constraints associated with the different slip systems are handled via an active set strategy borrowed from nonlinear programming theory. An algorithmic postprocessor satisfies exactly the plastic incompressibility constraint in situations of multislip, exploiting again the particular structure of the hyperelastic stress response of the model under consideration. The so-called consistent elastoplastic tangent moduli are derived in closed form and appear in the Eulerian geometric setting within a remarkably simple format. Furthermore, we discussed implementation of the coupled thermomechanical problem within the framework of an isothermal predictor and a heat conduction corrector algorithm based on the operator split methodology, yielding an algorithmic decoupling of the thermomechanical problem in a typical time step. Finally, the algorithmic framework has been successfully applied to two characteristic model problems of plane-strain single crystal plasticity.

Acknowledgement—I thank Professor L. Anand for his interest and helpful comments.

REFERENCES

Argyris, J. H. and Doltsinis, J. St. (1981). On the natural formulation and analysis of large deformation coupled thermomechanical problems. *Comput. Meth. Appl. Mech. Engng* **25**, 195–253.

Armero, F. and Simó, J. C. (1992). A new unconditionable stable fractional step method for nonlinear coupled thermomechanical problems. *Int. J. Numer. Meth. Engng* **35,** 737.
Asaro, R. J. (1979). Geometrical effects in the inhomogeneous deformation of ductile single crystals. *Acta Metall.* **27,** 445–453.
Asaro, R. (1983). Crystal plasticity. *J. Appl. Mech.* **50,** 921–934.
Asaro, R. J. and Needleman, A. (1985). Texture development and strain hardening in rate dependent polycrystals. *Acta Metall.* **33,** 923–953.
Becker, R. (1992). An analysis of shear localization during bending of a polycrystalline sheet. *J. Appl. Mech.* **59,** 491–496.
Bever, M. B., Holt, D. L. and Titchener, A. L. (1973). *The Stored Energy of Cold Work*, Pergamon, Oxford.
Borja, R. I. and Wren, J. R. (1993). Discrete micromechanics of elastoplastic crystals. *Int. J. Numer. Meth. Engng* **36,** 3815–3840.
Chang, Y. W. and Asaro, R. J. (1981). An experimental study of shear localization in aluminium-copper single crystals. *Acta Metall.* **29,** 241–257.
Cuitiño, A. M. and Ortiz, M. (1992). Computational modeling of single crystals. *Modelling Simul. Mat. Sci. Engng* **1,** 225–263.
Doltsinis, J. St. (1990). Aspects of modelling and computation in the analysis of metal forming. *Engng and Comput.* **7,** 2–20.
Duszek-Perzyna, M. K. and Perzyna, P. (1993). Adiabatic shear band localization in elastic–plastic single crystals. *Int. J. Solids Struct.* **30,** 61–89.
Eckart, E. (1948). The thermodynamics of irreversible processes: IV. The theory of elasticity and anelasticity. *Phys. Rev.* **73,** 337–382.
Flory, R. J. (1961). Thermodynamic relations for high elastic materials. *Trans. Faraday Soc.* **57,** 829–838.
Harren, S. V. and Asaro, R. (1989). Nonuniform deformations in polycrystals and aspects of the validity of the Taylor model. *J. Mech. Phys. Solids* **37,** 191–232.
Havner, K. S. (1982a). The theory of finite plastic deformation of crystalline solids. In *Mechanics of Solids, the Rodney Hill 60th Anniversary Volume* (Edited by H. G. Hopkins and M. J. Sewell), pp. 265–302. Pergamon, Swansea.
Havner, K. S. (1982b). Minimum plastic work selects the highest symmetry deformation in axially-loaded F.C.C. crystals. *Mech. Mater.* **1,** 97–111.
Hill, R. (1966). Generalized constitutive relations for incremental deformation of metal crystals by multislip. *J. Mech. Phys. Solids* **14,** 95–102.
Hill, R. and Havner, K. S. (1972). Perspective in the mechanics of elastoplastic crystals. *J. Mech. Phys. Solids* **30,** 5–22.
Hill, R. and Rice, J. R. (1972). Constitutive analysis of elasto-plastic crystals at arbitrary strain. *J. Mech. Phys. Solids* **20,** 401–413.
Kalidindi, S. R., Bronkhorst, C. A. and Anand, L. (1992). Crystallographic texture development in bulk deformation processing of FCC metals. *J. Mech. Phys. Solids* **40,** 537–569.
Kocks, U. F. (1970). The relation between polycrystal deformation and single crystal deformation. *Metall. Trans.* **1,** 1121–1143.
Koiter, W. T. (1960). General theorems of elastic–plastic solids. In *Progress in Solid Mechanics* (Edited by I. N. Sneddon and R. Hill). North Holland, Amsterdam.
Kratochvil, J. (1973). On a finite strain theory of elastic–inelastic materials. *Acta Mech.* **16,** 127–142.
Kröner, E. (1964). Plastizität und verzerrungen. In *Vorlesungen über Theoretische Physik* (Edited by A. Sommerfeld), p. 5. Auflage, Leipzig.
Kröner, E. and Teodosiu, C. (1972). Lattice defect approach to plasticity and viscoplasticity. In *Problems in Plasticity* (Edited by A. Sawczuk). Noordhoff, Gronige.
Lee, E. H. (1969). Elastic–plastic deformation of finite strains. *J. Appl. Mech. ASME* **36,** 1–6.
Luenberger, D. G. (1984). *Linear and Nonlinear Programming*. Addison-Wesley, Reading, MA.
Maier, G. (1970). A matrix structural theory of piecewise linear elastoplasticity with interacting yield planes. *Meccanica* **5,** 54–66.
Maier, G. and Grierson, D. (1979). *Engineering Plasticity and Mathematical Programming*. Pergamon Press, New York.
Mandel, J. (1972). *Plasticité Classique et Viscoplasticité. CISM Courses and Lectures*, no. 97. Springer, Berlin.
Mathur, K. K. and Dawson, P. R. (1989). On modeling the development of crystallographic texture in bulk forming processes. *Int. J. Plasticity* **5,** 67–94.
Miehe, C. (1994a). Aspects of the formulation and finite element implementation of large strain isotropic elasticity. *Int. J. Numer. Meth. Engng* **37,** 1981–2004.
Miehe, C. (1994b). On the representation of Prandtl-Reuss tensors within the framework of multiplicative elastoplasticity. *Int. J. Plasticity* **10,** 609–621.
Miehe, C. (1994c). Exponential map algorithm for stress updates in anisotropic multiplicative elastoplasticity for single crystals. *Int. J. Numer. Meth. Engng* (in press).
Miehe, C. (1995). Entropic thermoelasticity at finite strains. Aspects of the formulation and numerical implementation. *Comput. Meth. Appl. Mech. Engng* **120,** 243–269.
Miehe, C. and Stein, E. (1992). A canonical model of multiplicative elasto-plasticity. Formulation and aspects of the numerical implementation. *Euro. J. Mech. A/Solids* **11,** 25–43.
Mohan, R., Ortiz, M. and Shih, C. F. (1992). An analysis of cracks in ductile single crystals—I. Anti-plane shear, II. Mode I loading. *J. Mech. Phys. Solids* **40,** 291–313 and 315–337.
Needleman, A., Asaro, R. J., Lemonds, J. and Peirce, D. (1985). Finite element analysis of crystalline solids. *Comput. Meth. Appl. Mech. Engng* **52,** 689–708.
Peirce, D., Asaro, R. J. and Needleman, A. (1982). An analysis of nonuniform and localized deformation in ductile single crystals. *Acta Metall.* **30,** 1087–1119.
Peirce, D., Asaro, R. J. and Needleman, A. (1983). Material rate dependence and localized deformation in crystalline solids. *Acta Metall.* **31,** 1951–1976.

Perzyna, P. (1988). Temperature and rate dependent theory of plasticity of crystalline solids. *Rev. Phys. Appl.* **23,** 445–459.

Rashid, M. M. and Nemat-Nesser, S. (1992). A constitutive algorithm for rate-dependent crystal plasticity. *Comput. Meth. Appl. Mech. Engng* **94,** 201–228.

Rice, J. R. (1971). Inelastic constitutive relations for solids: an internal-variable theory and its application to metal plasticity. *J. Mech. Phys. Solids* **19,** 433–455.

Simó, J. C. and Armero, F. (1992). Geometrically nonlinear enhanced strain mixed methods and the method of incompatible modes. *Int. J. Numer. Meth. Engng* **33,** 1413–1449.

Simó, J. C., Kennedy, J. G. and Govindjee, S. (1988). Non-smooth multisurface plasticity and viscoplasticity. Loading/unloading conditions and numerical algorithms. *Int. J. Numer. Meth. Engng* **26,** 2161–2185.

Simó, J. C. and Miehe, C. (1992). Associative coupled thermoplasticity at finite strains: formulation, numerical analysis and implementation. *Comput. Meth. Appl. Mech. Engng* **98,** 41–104.

Spitzig, W. A. (1981). Deformation behaviour of nitrogenated Fe-Ti-Mn and Fe-Ti single crystals. *Acta Metall.* **29,** 1359–1377.

Steinmann, P. and Stein, E. (1996). On the numerical treatment and analysis of finite deformation single crystal plasticity. *Comput. Meth. Appl. Mech. Engng* **129,** 235–254.

Taylor, G. I. and Quinney, M. A. (1933). The latent energy remaining in a metal after cold working. *Proc. R. Soc. Lond.* **A143,** 307.

Teodosiu, C. (1970). A dynamic theory of dislocations and its applications to the theory of the elastic–plastic continuum. In *Fundamental Aspects of Dislocation Theory* (Edited by J. A. Simmons *et al.*), Vol. II, pp. 837–876. National Bureau of Standards (U.S.) Special Publication.

Teodosiu, C. and Sidoroff, F. (1976). A finite theory of the elastoviscoplasticity of single crystals. *Int. J. Engng Sci.* **14,** 713–723.

Zienkiewicz, O. C. and Taylor, R. L. (1989). *The Finite Element Method*, Vol. 1. McGraw-Hill, London.